European Journal of Pharmaceutics and Biopharmaceutics 85 (2013) 177–183

Contents lists available at SciVerse ScienceDirect

European Journal of Pharmaceutics and Biopharmaceutics

journal homepage: www.elsevier.com/locate/ejpb

Research paper

Impact of heat treatment on miscibility of proteins and disaccharides in frozen solutions

Ken-ichi Izutsu [a,*], Chikako Yomota [a], Haruhiro Okuda [a], Toru Kawanishi [a], Theodore W. Randolph [b], John F. Carpenter [c]

[a] National Institute of Health Sciences, Tokyo, Japan
[b] Department of Chemical and Biological Engineering, University of Colorado, Boulder, CO, USA
[c] Department of Pharmaceutical Sciences, University of Colorado Denver, Aurora, CO, USA

ARTICLE INFO

Article history:
Available online 18 May 2013

Keywords:
Protein formulation
Stability
Phase separation
Freeze-concentration
Heat treatment
Freeze-drying

ABSTRACT

The purpose of this study was to elucidate the effect of heat treatment (annealing) on the miscibility of concentrated protein and disaccharide mixtures in the freezing segment of lyophilization. Frozen solutions containing a protein (e.g., recombinant human albumin, chicken egg lysozyme, bovine plasma immunoglobulin G, or a humanized IgG1k monoclonal antibody) and a non-reducing disaccharide (e.g., sucrose or trehalose) showed single thermal transitions of the solute mixtures (glass transition temperature of maximally freeze-concentrated solutes: T_g') in their first heating scans. Heat treatment (e.g., −5 °C, 30 min) of some disaccharide-rich mixture frozen solutions at temperatures far above their T_g' induced two-step T_g' transitions in the subsequent scans, suggesting the separation of the solutes into concentrated protein–disaccharide mixture phase and disaccharide phase. Other frozen solutions showed a single transition of the concentrated solute mixture both before and after heat treatment. The apparent effects of the heat treatment temperature and time on the changes in thermal properties suggest molecular reordering of the concentrated solutes from a kinetically fixed mixture state to a more thermodynamically favorable state as a result of increased mobility. The implications of these phenomena on the quality of protein formulations are discussed.

1. Introduction

The commercial development of recombinant protein pharmaceuticals requires rational formulation design to retain protein stability throughout the production process and clinical use [1,2]. Freeze-drying is an effective method of achieving an acceptable shelf life (e.g., 24 months) for chemically and/or physically unstable proteins. While the removal of water by lyophilization reduces the rate of protein chemical degradation during storage, the process often induces irreversible protein aggregation due to higher-order structural changes. The structurally-altered protein molecules are also more susceptible to various types of chemical degradation during storage [3]. To prevent the lyophilization-induced protein unfolding, many protein formulations contain non-reducing disaccharides (e.g., sucrose and trehalose) that substitute surrounding water molecules and provide a glassy matrix, which is required for long-term protein storage stability in dried solids [1,4]. Low-molecular-weight saccharides reduce protein denaturation in aqueous solutions and during freezing because they are preferentially excluded from the surface of the proteins; they also increase the free energy of protein unfolding by elevating the chemical potential of the unfolded state above that of the native state [5–7]. The increasing clinical relevance of lyophilized protein pharmaceuticals highlights the importance of understanding various factors that determine the formulation quality and the efficiency of the typical long high-energy process.

In the first step of lyophilization, freezing to form crystals of pure water concentrates the remaining solutes into a highly viscous solution [8,9]. Some solutes tend to crystallize in frozen solutions, while others are kinetically trapped in the concentrated supercooled liquids. Multiple solutes in lyophilized pharmaceutical formulations can be miscible or immiscible in the freeze-concentrates, depending on the particular combination, concentration ratio, and freezing process [10–16]. The multiple concentrated solute phases should form during the freezing process and upon exposure of the frozen solutions to higher temperatures. Freeze-concentration separates some polymer combinations, such as dextran and polyvinylpyrrolidone (PVP) or ovalbumin and PVP (in the presence of NaCl), from miscible lower-concentration aqueous solutions into multiple non-crystalline phases rich in one of the polymers by the same thermodynamic mechanism that induces aqueous two-layer

* Corresponding author. National Institute of Health Sciences, Kamiyoga 1-18-1, Setagaya 158-8501, Tokyo, Japan. Tel.: +81 337001141; fax: +81 337076950.
E-mail address: izutsu@nihs.go.jp (K.-i. Izutsu).

0939-6411/$ - see front matter © 2013 Elsevier B.V. All rights reserved.
http://dx.doi.org/10.1016/j.ejpb.2013.05.004

systems [10,14,16,17]. This phase separation influences the physical properties of the frozen solutions and the resulting material post-drying (e.g., multiple transitions and varied propensity for physical collapse) [18,19]. Many other formulation ingredients tend to be freeze-concentrated without these apparent phase separations [20].

The miscibility of proteins and non-reducing disaccharides in frozen solutions and freeze-dried solids is of particular interest in formulation development. Several preceding studies utilizing thermal analysis and spectroscopic methods (e.g., Raman and near-infrared mapping, FT-IR) suggest non-ideal mixing of proteins and disaccharides in freeze-dried solids; however, available information is still limited partly because of the microporous and hygroscopic nature of these cakes [13,20–27]. Raman microscopy analysis of frozen solutions also revealed variable distributions of lysozyme and trehalose in freeze-concentrated liquid and ice regions [28]. Our previous study indicated contribution of thermal history on the miscibility of some solutes in frozen solutions [25]. For example, a nonionic polymer (e.g., dextran) and a disaccharide (e.g., trehalose) that are initially concentrated into a mixture supercooled phase upon ice formation, separate into saccharide-rich and solute mixture freeze-concentrated phases upon heat treatment of frozen solutions at temperatures far above the glass transition temperature of maximally freeze-concentrated solutes (T'_g). The composition of solutes in the resulting non-crystalline phases depends largely on the consisting polymers. The post-freezing heat treatment (i.e., annealing) is gaining increasing attention as a method for reducing the ice-subliming primary drying segment time and also the inter-batch and inter-vial heterogeneity in drying behavior. The ice crystal size growth by coalescence (Ostwald ripening) and the resulting larger connecting pores in the dried solid layers often facilitate faster ice sublimation. The method would be particularly valuable for drying biopharmaceutical formulations since many disaccharide-containing frozen solutions have a relatively low "maximum allowable product temperature" to avoid the physical collapse of the products [29].

There is a reasonable chance that the increasing solute mobility during exposure of frozen solutions to temperatures far above the T'_g alters the miscibility of the concentrated proteins and disaccharides. Therefore, in the present study, we performed thermal analysis to investigate the effects of heat treatment on the miscibility of proteins and disaccharides in frozen solutions. Recombinant human albumin, egg yolk lysozyme, bovine immunoglobulin G, and a humanized monoclonal antibody were used as model proteins. Temperature profiles of the thermal transition (T'_g) provided valuable information on solute miscibility in freeze-concentrates.

2. Materials and methods

2.1. Materials

All chemicals employed in this study were of analytical grade and were obtained from the following commercial sources: sucrose, D-(+)-trehalose dihydrate, and recombinant human albumin (rHA, A9731; Sigma–Aldrich, St. Louis, MO); bovine plasma immunoglobulin G (bIgG, 641401; MP Biomedicals, Solon, OH); L-histidine, L-histidine hydrochloride monohydrate, disodium hydrogenphosphate, and sodium dihydrogenphosphate dihydrate (Wako Pure Chemical Industries, Osaka, Japan); and egg yolk lysozyme (Seikagaku, Tokyo, Japan). A commercial recombinant DNA-derived humanized IgG1k monoclonal antibody (mAbA) lyophilized formulation was also used in the study. The bIgG and mAbA were dialyzed overnight against a histidine-HCl buffer (5 mM, pH 7.0) containing 100 mM NaCl. Other proteins were dialyzed against the buffer without NaCl. The concentrations of the proteins were determined from the absorbance at 280 nm by using the appropriate extinction coefficient for each protein.

2.2. Thermal analysis of frozen solutions and freeze-dried solids

Thermal analysis of the frozen solutions was performed using a differential scanning calorimeter (DSC Q-10; TA Instruments, New Castle, DE) and Universal Analysis software (TA Instruments). All solutions used in the thermal analysis were single-phase at room temperature. Aliquots of aqueous solutions (10 μL) in aluminum cells were cooled from room temperature to −70 °C at 10 °C/min. The first heating scan of the frozen solutions at 5 °C/min was paused at various temperatures (−25 to −5 °C, −5 °C unless otherwise mentioned) and then maintained at the temperature for various times (1–480 min, 30 min unless otherwise mentioned). After annealing, the solutions were cooled to −70 °C and then heated at a rate of 5 °C/min. The first derivative of the thermograms was calculated to increase the sensitivity of detection of the thermal events (e.g., T'_g). The T'_g was estimated as the temperature at which the highest peak in the derivative thermogram appeared. The two-step heat flow changes observed in the first and second scans of some heat-treated frozen solutions were provisionally described as lower- (T'_{g1L}, T'_{g2L}) and higher temperature (T'_{g1H}, T'_{g2H}) transitions.

3. Results

3.1. Effects of heat treatment on albumin and disaccharide miscibility

Fig. 1 shows the derivative thermograms of frozen solutions containing rHA and trehalose at various concentration ratios (total 200 mg/mL) obtained in the heating scans prior to and after heat treatment at −5 °C for 30 min. An exotherm attributed to ice crystallization was observed during cooling between −15 and −25 °C (data not shown). The frozen trehalose solution showed a peak that

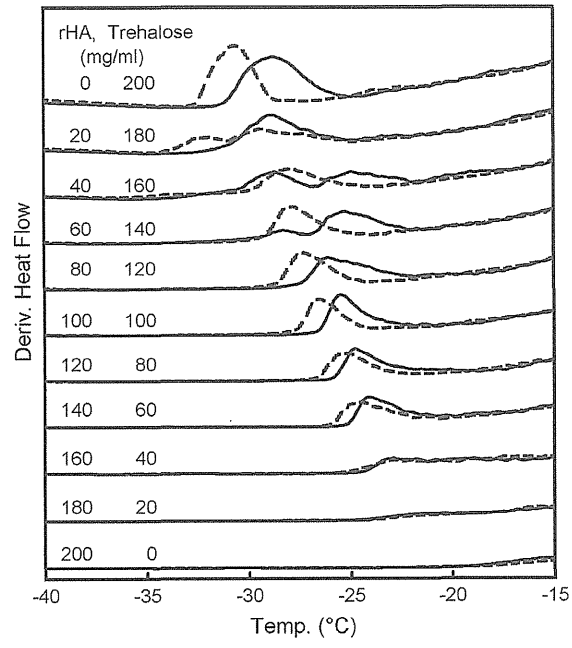

Fig. 1. Derivative thermograms of frozen solutions containing various concentration ratios of rHA and trehalose (total 200 mg/mL, 5 mM histidine-HCl buffer, pH 7.0, 10 μL) obtained in the heating scans (5 °C/min) prior to (first scans, dotted lines) and after (second scans, solid lines) heat treatment at −5 °C for 30 min.

indicates a heat capacity change at −30.6 °C (T'_g) in the first scan. The second scan of the frozen solution shifted the transition to a slightly higher temperature (1–3 °C), suggesting further concentration of the solutes upon heat treatment. The frozen solutions containing rHA only or higher concentrations of rHA did not exhibit apparent T'_g transitions in the scans both before and after the heat treatment, as reported in other protein solutions [16,30]. The gradual endothermic shift of the thermogram from approximately −23 °C suggests continuous physical property changes (e.g., melting of surrounding ice) of the freeze-concentrated protein solutions. Analysis using other methods often produces T'_g values of frozen protein solutions ranging from −12 to −8 °C [30]. These frozen solutions also showed smaller thermal transitions at −50 to −40 °C (data not shown). While the origin of the thermal event is under active discussions, the broad nature of these lower temperature transitions prevented detailed analysis in this study [31].

Most of the trehalose-rich and equivalent concentrations of rHA and trehalose mixture frozen solutions exhibited single T'_g transitions that suggested mixing of the freeze-concentrated solutes at varied temperatures during the first scans. However, a frozen trehalose-dominant solution (i.e., 20 mg/mL rHA, 180 mg/mL trehalose) showed two peaks at the T'_g temperature range found in the first scan. Heat treatment of some trehalose-rich frozen solutions (e.g., 40 mg/mL rHA, 160 mg/mL trehalose) at −5 °C (30 min) induced two transition peaks in the subsequent heating scans. The relative magnitude of the higher temperature transition, as indicated by the area under the peak of the first derivative curve, increased with increasing rHA concentration ratio. Annealing only slightly (up to 2 °C) shifted the single transition in other frozen solutions. The single and double peaks should indicate T'_g transitions of the miscible and phase-separated concentrated phases that differ in the solute compositions. Broad single peaks in the boundary concentration ratio solutions (e.g., 80 mg/mL rHA, 120 mg/mL trehalose) suggest the overlapping of the multiple transitions upon heat treatment. Changing the buffer from 5 mM histidine-HCl to 10 mM sodium phosphate (pH 7.0) did not apparently alter the thermal properties of the heat-treated rHA and trehalose mixture frozen solutions (data not shown).

The effects of the heat treatment temperature and time on the thermal properties of the frozen rHA (40 mg/mL) and trehalose

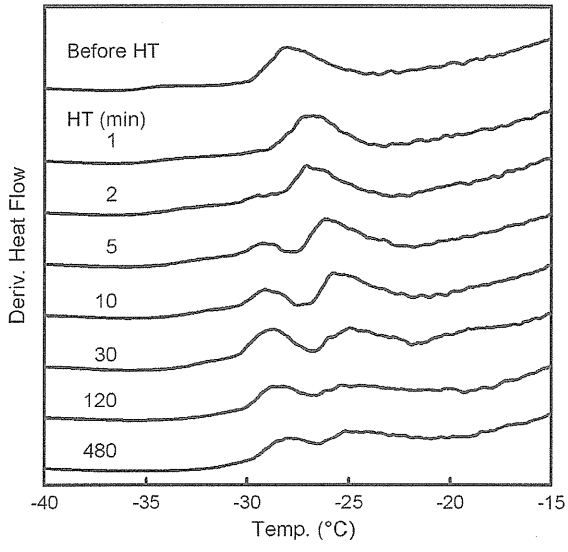

Fig. 2. Derivative thermograms of frozen solutions containing 40 mg/mL rHA and 160 mg/mL trehalose (5 mM histidine-HCl buffer, pH 7.0, 10 μL) obtained in the heating scans (5 °C/min) prior to and after heat treatment at −5 °C for 1–480 min.

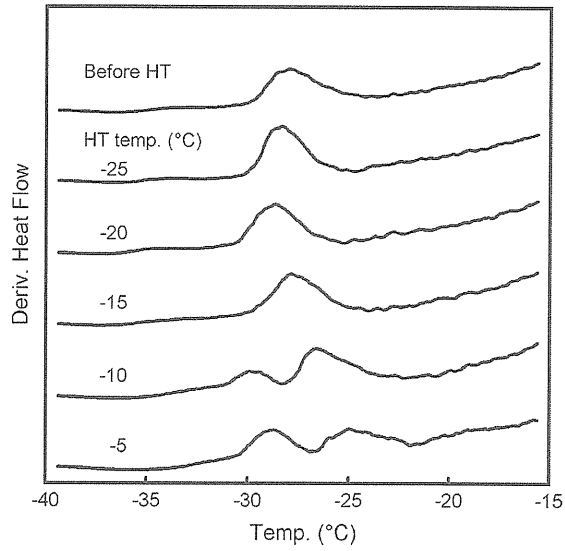

Fig. 3. Derivative thermograms of frozen solutions containing 40 mg/mL rHA and 160 mg/mL trehalose (5 mM histidine-HCl buffer, pH 7.0, 10 μL) obtained in the heating scans (5 °C/min) prior to and after heat treatment at −25 °C to −5 °C for 30 min.

(160 mg/mL) mixture solutions were studied. Fig. 2 shows the derivative thermograms obtained in the scans prior to and after the heat treatment at −5 °C for 1–480 min. The frozen solutions retained the single T'_g after the shorter heat treatments, whereas longer exposure to the elevated temperature resulted in two transitions at approximately −28 and −25 °C in the subsequent heating scan. Further holding at −5 °C resulted in the broadening of the two transition peaks. Heat treatment at −25 to −5 °C resulted in apparent changes in the thermal properties at higher temperatures (−10 °C<, 30 min) (Fig. 3). Some frozen solutions exhibited slower phase separation when annealed at the lower temperature (−15 °C, 120, and 480 min, data not shown). The apparent effect of the heat treatment temperature and time indicates the contribution of the increasing solute mobility at temperatures far above T'_g to the solute miscibility change. The 100 mg/mL rHA and trehalose mixture frozen solution retained the single T'_g peak even with long heat treatment times (e.g., −5 °C, 480 min), indicating practical stability of the freeze-concentrated mixture (data not shown).

Various protein and disaccharide mixture frozen solutions were subjected to thermal analysis at different weight concentration ratios to examine the effects of heat treatment (Fig. 4). Some frozen solutions showed single or no apparent transitions. The profiles of the transition temperatures obtained in the heating scans prior to and after the heat treatment (−5 °C, 30 min) revealed similar physical property changes of the systems that depend largely on the concentration ratio. Heat-treated trehalose-rich rHA and trehalose mixture solutions (total 100 and 200 mg/mL) exhibited their lower temperature transitions (T'_{g2L}) close to that of single-solute frozen trehalose solution (approximately −30 °C), which should indicate the transition of the phase dominant in trehalose. The higher temperature event (T'_{g2H}) always appeared at around −25 °C, indicating that a phase of constant composition formed post-annealing irrespective of the initial solution composition. In addition, the plots of T'_g vs. the disaccharide mass fraction suggest that the extent of the phase separation is minimal when the mass fractions are 0.5 or lower. The threshold of the T'_g profiles suggests that the solute mixture phase retains up to 1:1 disaccharide/protein weight concentration ratios of rHA and trehalose upon heat treatment. The relative contribution of the solute compositions to the

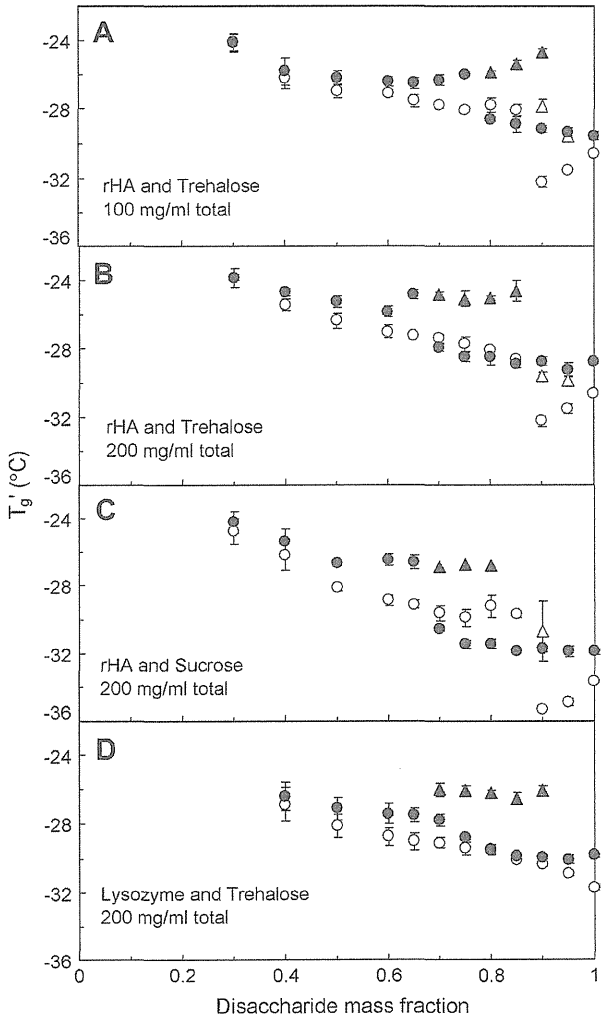

Fig. 4. Transition temperature profiles of frozen protein (rHA, lysozyme) and disaccharide (trehalose, sucrose) mixture frozen solutions (10 μL) obtained in the heating scans (5 °C/min) prior to (T'_{g1L}: ○, T'_{g1H}: △) and after (T'_{g2L}: ●, T'_{g2H}: ▲) heat treatment at −5 °C for 30 min. The total concentration of protein and disaccharide was 100 or 200 mg/mL (n = 3, average ± s.d.).

annealing-induced changes in miscibility was compared at two different compositions (total concentrations of 100 and 200 mg/mL). Other disaccharide-rich mixture frozen solutions of protein and disaccharides (e.g., rHA and sucrose, lysozyme and trehalose) also exhibited the two T'_g upon heat treatment. The lower intrinsic transition temperature of sucrose relative to that of trehalose should also lower the T'_g of the two phases. The transition temperature profiles were similar to those of dextran and disaccharides observed in a previous study [25].

The effect of NaCl, which is often included in lyophilized formulations for protein solubilization or to provide physiological osmolarity, on the thermal properties of rHA and trehalose mixtures was studied. Fig. 5 shows the derivative thermograms of frozen solutions containing 40 mg/mL rHA, 160 mg/mL trehalose, and 0–250 mM NaCl obtained prior to and after heat treatment at −5 °C for 30 min. The salt lowered the single transition temperature obtained in the first heating scans, presumably because of the plasticizing effect [32]. Higher concentrations of salt lowered and broadened the two T'_g transitions of the heat-treated frozen solutions, suggesting the distribution of the salt to the miscible and phase-separated freeze-concentrated phases.

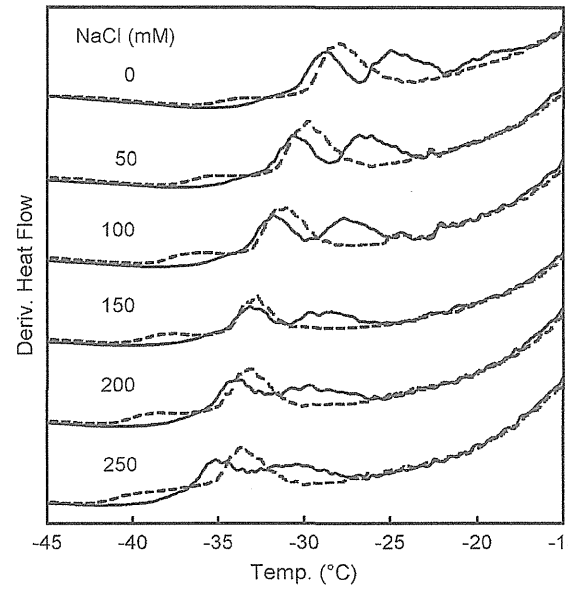

Fig. 5. Effect of various concentrations of NaCl (0–250 mM) on the derivative thermograms of frozen solutions containing 40 mg/mL recombinant human albumin and 160 mg/mL trehalose obtained in the heating scans (5 °C/min) prior to (dotted lines) and after (solid lines) heat treatment at −5 °C for 30 min.

3.2. Effects of heat treatment on immunoglobulin and disaccharide miscibility

The effects of post-freezing heat treatment were also studied in the solutions containing an immunoglobulin (i.e., bovine plasma IgG and recombinant humanized IgG1k monoclonal antibody) and trehalose in the presence of NaCl and the pH buffer salt. The disaccharide-rich mixture frozen solutions (20–60 mg/mL bIgG, 140–180 mg/mL trehalose) exhibited the two T'_g transitions upon

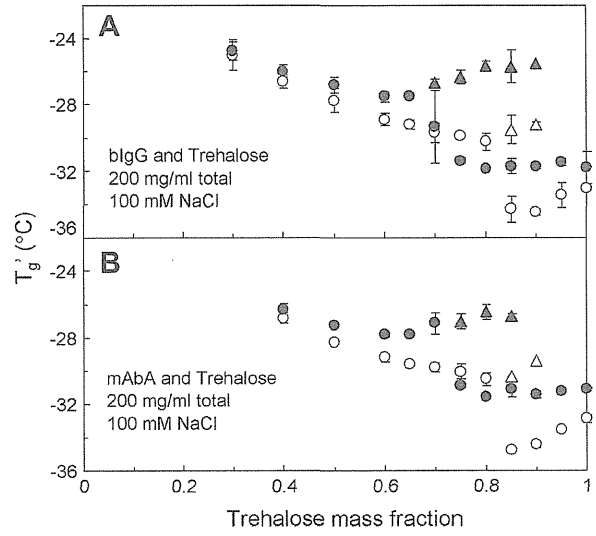

Fig. 6. Transition temperature profiles of frozen solutions containing an immunoglobulin (bIgG, mAbA), trehalose, NaCl (100 mM), and histidine-HCl buffer (5 mM, pH 7.0, 10 μL) obtained in the heating scans (5 °C/min) prior to (T'_{g1L}: ○, T'_{g1H}: △) and after (T'_{g2L}: ●, T'_{g2H}: ▲) heat treatment at −5 °C for 30 min. The total concentration of immunoglobulin and trehalose was 200 mg/mL (n = 3, average ± s.d.).

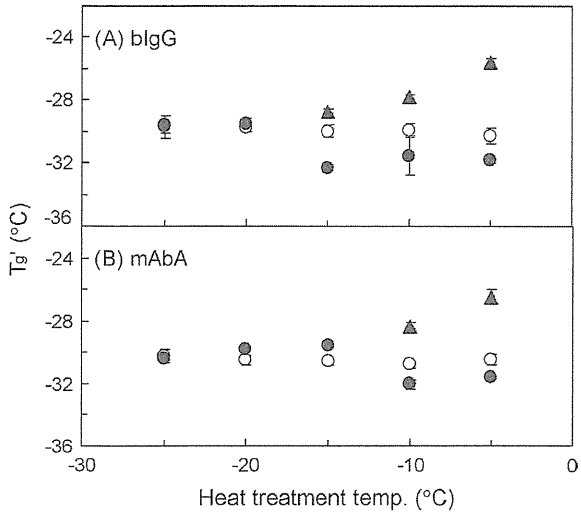

Fig. 7. Effect of heat treatment temperature on the T'_g of frozen solutions containing an immunoglobulin (bIgG, mAbA, 40 mg/mL), trehalose (160 mg/mL), 100 mM NaCl, and 5 mM histidine-HCl buffer (pH 7.0) obtained in the heating scans (5 °C/min) prior to (T'_{g1}: ○) and after (T'_{g2L}: ●, T'_{g2H}: ▲) heat treatment at −25 to −5 °C for 30 min ($n = 3$, average ± s.d.).

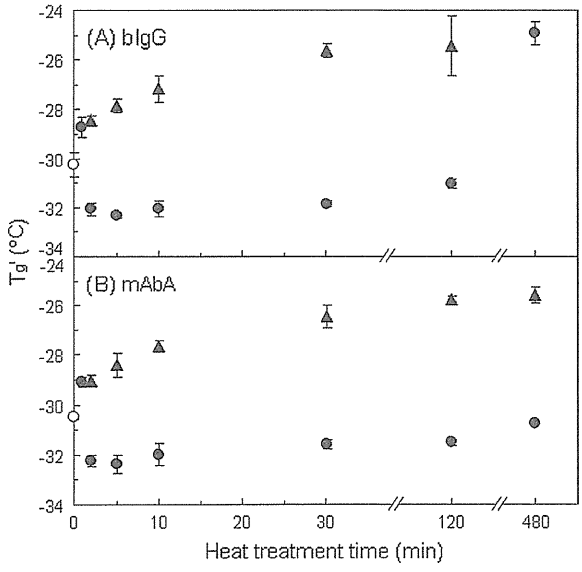

Fig. 8. Effect of heat treatment time on the T'_g of frozen solutions containing an immunoglobulin (bIgG, mAbA, 40 mg/mL), trehalose (160 mg/mL), 100 mM NaCl, and 5 mM histidine-HCl buffer (pH 7.0) obtained in the heating scans (5 °C/min) prior to (T'_{g1}: ○) and after (T'_{g2L}: ●, T'_{g2H}: ▲) heat treatment at −5 °C ($n = 3$, average ± s.d.).

heat treatment at −5 °C for 30 min (Fig. 6). In contrast, the heat treatment only slightly shifted the transition of frozen solutions containing equivalent concentrations of bIgG and trehalose to higher temperatures. No thermal transitions indicative of either the crystallization or melting of NaCl dihydrate-ice were observed over the concentration range employed in the experiments.

Figs. 7 and 8 show the effects of heat treatment temperature and time on the transition temperatures of the frozen immunoglobulin and trehalose mixture solutions (e.g., 40 mg/mL bIgG or mAbA, 160 mg/mL trehalose, 100 mM NaCl, 5 mM L-histidine buffer). The frozen solution showed the two T'_g transitions upon longer and higher temperature heat treatment as observed in the albumin systems. The systems containing trehalose and the two immunoglobulins exhibited similar propensity for the annealing-induced solute phase separation. The lower temperature transition (T'_{g2L}) became broad and unclear with longer heat treatments (>120 min) of the frozen solutions (data not shown). The gradual changes of thermograms observed after longer heat treatments suggest continuous changes in the phase composition in NaCl-containing systems.

4. Discussion

The post-freeze heat treatment induced phase separation of some protein and disaccharide mixture systems relevant for pharmaceutical formulations. The higher transition temperature phase should contain the protein and disaccharide molecules [25]. When the composition of protein–disaccharide solutions exceeds a certain ratio, phase separation leads to the formation of disaccharide-rich and protein-rich phases, which correspond to lower and higher T'_g events observed during heating post-annealing. Clarifying the mechanism of the phenomena and its effect on the formulation quality should assist rational design and manufacturing of lyophilized pharmaceuticals.

4.1. Possible mechanism of the annealing-induced solute phase separation

Freezing many multi-solute aqueous solutions, which often starts from −5 to −25 °C, concentrates the solutes into highly viscous supercooled solutions surrounding ice crystals in relatively short time periods. Our studies indicated two mechanisms that induce multiple non-crystalline concentrated solute phases in a frozen solution. The increasing concentrations during the ice growth separate some polymer systems (e.g., PVP and dextran) into multiple supercooled phases rich in one of the component polymers, resulting in two T'_g transition peaks in the following heating scans [14,33]. Cooling other systems, including those containing disaccharides and proteins, should kinetically trap the solutes in a highly viscous miscible phase, which exhibits a single T'_g. On annealing of disaccharide-rich compositions above their T'_g, an increase in the mobility within the freeze concentrate should facilitate a separation into thermodynamically favorable disaccharide-rich and protein-rich phases. In addition, a decrease in the viscosity could enable limited ice crystallization (i.e., devitrification) during annealing. On the contrary, annealing should keep some protein-rich and equivalent concentration ratio mixtures in the single concentrated phase.

The cause of the two transitions obtained in the first scans of some disaccharide-dominant mixture frozen solutions (10–30 mg/mL rHA, 170–190 mg/mL disaccharide) remains unclear. Our preliminary experiments suggest that the solution volume and cooling speed also influence the thermal behavior of the solutions during warming (data not shown). The relationship between the thermal analysis conditions and physical properties of frozen solutions remains to be elucidated.

4.2. Factors determining protein and disaccharide miscibility

The solute miscibility in the freeze-concentrates may depend on the magnitude and nature of protein-excipient, protein–protein, and excipient–excipient interactions in the hydrated environment (e.g., hydrogen bonding, hydrophobic interactions, and van der Waals interactions). Factors that influence these interactions include protein and excipient structure, solute concentration in the

unfrozen fraction, and other solution conditions such as temperature, ionic strength, pH, and the type of salt [14,16,34,35]. When excipient–excipient interactions are more favorable than protein–excipient interactions, phase separation may occur. The proteins and disaccharides are suggested to be mixed up to approximately 1:1 disaccharide/protein weight concentration ratio after heat treatment (Figs. 4 and 6). This ratio is consistent with the reported maximum ratio of disaccharides interacting directly with the protein molecules in the freeze-dried solids obtained experimentally through spectroscopic methods, water–vapor sorption measurement, and molecular modeling approaches based on the number of hydrogen bonds [36–38].

4.3. Implications in pharmaceutical lyophilization

The annealing-induced post-freezing phase separation should affect the stability of proteins during the formulation process and subsequent storage in various ways. Many freeze-dried antibody formulations contain 1:1 or 1:2 mass ratio of protein and disaccharide. The results suggest that the ingredients in these formulations separate into multiple phases or remain miscible upon annealing of the frozen solutions depending largely on the composition. Possible difference in the thermal history of the small thermal analysis solutions and solutions in formulation vials should affect the occurrence of the phase separation. The disaccharide molecules in the solute mixture phase should maintain the hetero-molecular hydrogen bonding that substitute water molecules. It, however, remains unclear whether the excipients provide sufficient interaction to protect the protein conformation throughout the process and during storage [39–42]. Possible changes in the local environment, including the co-solute compositions (e.g., inorganic salts and pH modifiers) and their mobility in the mixture phase, should alter the protein stability. Lower transition temperatures of the disaccharide phase in the frozen solutions and dried solids can adversely affect physical and chemical stability of the system during the process and subsequent storage. Freeze-drying of the phase-separated frozen solutions should also require appropriate process control to ensure the efficient ice sublimation and physical integrity of the resulting solids [43–45].

5. Conclusion

In this study, we found that sucrose and trehalose, which are the most commonly used excipients in lyophilized therapeutic protein formulations, and proteins can undergo post-freeze annealing-induced phase separation. The increasing mobility of solutes and melting of surrounding ice during heat treatment should allow spatial reordering of the freeze-concentrated proteins and disaccharides toward more thermodynamically stable states. The results clearly indicate that the application of post-freeze annealing requires sufficient understanding of its effects on the quality of products, including protein stability during processing and storage. In conclusion, the phase separation of protein and disaccharide combinations in frozen solutions should be considered an important factor when developing freeze-dried formulations.

Acknowledgement

This work was supported in part by the Japan Health Sciences Foundation.

References

[1] M.J. Pikal, Mechanism of protein stabilization during freeze-drying and storage: the relative importance of thermodynamic stabilization and glassy state relaxation dynamics, in: L. Rey, J.C. May (Eds.), Freeze-drying/Lyophilization of Pharmaceutical and Biological Products, Marcel Dekker, New York, 1999, pp. 161–198.
[2] J.F. Carpenter, K. Izutsu, T.W. Randolph, Freezing- and drying-induced perturbations of protein structure and mechanisms of protein protection by stabilizing additives, in: L. Rey, J.C. May (Eds.), Freeze-drying/Lyophilization of Pharmaceutical and Biological Products, Marcel Dekker, New York, 1999, pp. 123–160.
[3] B.S. Chang, R.M. Beauvais, A. Dong, J.F. Carpenter, Physical factors affecting the storage stability of freeze-dried interleukin-1 receptor antagonist: glass transition and protein conformation, Arch. Biochem. Biophys. 331 (1996) 249–258.
[4] J.F. Carpenter, J.H. Crowe, An infrared spectroscopic study of the interactions of carbohydrates with dried proteins, Biochemistry 28 (1989) 3916–3922.
[5] S.N. Timasheff, Stabilization of protein structure by solvent additives, in: T. Ahern, M.C. Manning (Eds.), Stability of Protein Pharmaceuticals, Plenum, New York, 1992, pp. 265–285.
[6] T. Arakawa, S.J. Prestrelski, W.C. Kenney, J.F. Carpenter, Factors affecting short-term and long-term stabilities of proteins, Adv. Drug Deliv. Rev. 46 (2001) 307–326.
[7] S. Ohtake, Y. Kita, T. Arakawa, Interactions of formulation excipients with proteins in solution and in the dried state, Adv. Drug Deliv. Rev. 63 (2011) 1053–1073.
[8] A.P. MacKenzie, Non-equilibrium freezing behaviour of aqueous systems, Philos. Trans. R. Soc. Lond. B 278 (1971) 167–189.
[9] H. Levine, L. Slade, Thermomechanical properties of small-carbohydrate–water glasses and 'rubbers', J. Chem. Soc. Faraday Trans. 1 (84) (1988) 2619–2633.
[10] L.M. Her, M. Deras, S.L. Nail, Electrolyte-induced changes in glass transition temperatures of freeze-concentrated solutes, Pharm. Res. 12 (1995) 768–772.
[11] M.C. Heller, J.F. Carpenter, T.W. Randolph, Effects of phase separating systems on lyophilized hemoglobin, J. Pharm. Sci. 85 (1996) 1358–1362.
[12] K. Izutsu, S. Yoshioka, S. Kojima, T.W. Randolph, J.F. Carpenter, Effects of sugars and polymers on crystallization of poly(ethylene glycol) in frozen solutions: phase separation between incompatible polymers, Pharm. Res. 13 (1996) 1393–1400.
[13] T.W. Randolph, Phase separation of excipients during lyophilization: effects on protein stability, J. Pharm. Sci. 86 (1997) 1198–1203.
[14] K. Izutsu, M. Heller, T.W. Randolph, J.F. Carpenter, Effect of salts and sugars on phase separation of polyvinylpyrrolidone-dextran solutions induced by freeze-concentration, J. Chem. Soc. Faraday Trans. 94 (1998) 411–418.
[15] M.C. Heller, J.F. Carpenter, T.W. Randolph, Application of a thermodynamic model to the prediction of phase separations in freeze-concentrated formulations for protein lyophilization, Arch. Biochem. Biophys. 363 (1999) 191–201.
[16] K. Izutsu, S. Kojima, Freeze-concentration separates proteins and polymer excipients into different amorphous phases, Pharm. Res. 17 (2000) 1316–1322.
[17] K. Izutsu, C. Yomota, T. Kawanishi, Impact of heat treatment on the physical properties of noncrystalline multisolute systems concentrated in frozen aqueous solutions, J. Pharm. Sci. 100 (2011) 5244–5253.
[18] N. Perez-Moral, C. Adnet, T.R. Noel, R. Parker, The aggregative stability of β-lactoglobulin in glassy mixtures with sucrose, trehalose and dextran, Eur. J. Pharm. Biopharm. 78 (2011) 264–270.
[19] B.S. Bhatnagar, S.W. Martin, T.S. Hodge, T.K. Das, L. Joseph, D.L. Teagarden, E.Y. Shalaev, R. Suryanarayanan, Investigation of PEG crystallization in frozen and freeze-dried PEGylated recombinant human growth hormone-sucrose systems: implications on storage stability, J. Pharm. Sci. 100 (2011) 3062–3075.
[20] S.L. Shamblin, L.S. Taylor, G. Zografi, Mixing behavior of colyophilized binary systems, J. Pharm. Sci. 87 (1998) 694–701.
[21] A.M. Padilla, I. Ivanisevic, Y. Yang, D. Engers, R.H. Bogner, M.J. Pikal, The study of phase separation in amorphous freeze-dried systems. Part I: Raman mapping and computational analysis of XRPD data in model polymer systems, J. Pharm. Sci. 100 (2011) 206–222.
[22] L.S. Taylor, G. Zografi, Sugar–polymer hydrogen bond interactions in lyophilized amorphous mixtures, J. Pharm. Sci. 87 (1998) 1615–1621.
[23] N. Jovanović, A. Gerich, A. Bouchard, W. Jiskoot, Near-infrared imaging for studying homogeneity of protein–sugar mixtures, Pharm. Res. 23 (2006) 2002–2013.
[24] D.S. Katayama, J.F. Carpenter, K.P. Menard, M.C. Manning, T.W. Randolph, Mixing properties of lyophilized protein systems: a spectroscopic and calorimetric study, J. Pharm. Sci. 98 (2009) 2954–2969.
[25] K. Izutsu, C. Yomota, T. Kawanishi, Impact of heat treatment on the physical properties of noncrystalline multisolute systems concentrated in frozen aqueous solutions, J. Pharm. Sci. 100 (2011) 5244–5253.
[26] A.M. Padilla, M.J. Pikal, The study of phase separation in amorphous freeze-dried systems, Part 2: Investigation of Raman mapping as a tool for studying amorphous phase separation in freeze-dried protein formulations, J. Pharm. Sci. 100 (2011) 1467–1474.
[27] V. Ragoonanan, A. Aksan, Heterogeneity in desiccated solutions: implications for biostabilization, Biophys. J. 94 (2008) 2212–2227.
[28] J. Dong, A. Hubel, J.C. Bischof, A. Aksan, Freezing-induced phase separation and spatial microheterogeneity in protein solutions, J. Phys. Chem. B 113 (2009) 10081–10087.
[29] M.J. Akers, V. Vasudevan, M. Stickelmeyer, Formulation development of protein dosage forms, Pharm. Biotechnol. 14 (2002) 47–127.
[30] B.S. Chang, C.S. Randall, Use of subambient thermal analysis to optimize protein lyophilization, Cryobiology 29 (1992) 632–656.

[31] A. Pyne, R. Suryanarayanan, The effect of additives on the crystallization of cefazolin sodium during freeze-drying, Pharm. Res. 20 (2003) 283–291.
[32] S.L. Nail, S. Jiang, S. Chongprasert, S.A. Knopp, Fundamentals of freeze-drying, Pharm. Biotechnol. 14 (2002) 281–360.
[33] K. Izutsu, N. Aoyagi, S. Kojima, Effect of polymer size and cosolutes on phase separation of poly(vinylpyrrolidone) (PVP) and dextran in frozen solutions, J. Pharm. Sci. 94 (2005) 709–717.
[34] B.Y. Zaslavsky, Aqueous Two-phase Partitioning, Marcel Dekker, New York, 1995.
[35] V. Tolstoguzov, Compositions and phase diagrams for aqueous systems based on proteins and polysaccharides, Int. Rev. Cytol. 192 (2000) 3–31.
[36] B. Wang, S. Tchessalov, N.W. Warne, M.J. Pikal, Impact of sucrose level on storage stability of proteins in freeze-dried solids: I. Correlation of protein–sugar interaction with native structure preservation, J. Pharm. Sci. 98 (2009) 3131–3144.
[37] K.R. Ward, G.D. Adams, H.O. Alpar, W.J. Irwin, Protection of the enzyme L-asparaginase during lyophilisation – a molecular modelling approach to predict required level of lyoprotectant, Int. J. Pharm. 187 (1999) 153–162.
[38] L.L. Chang, D. Shepherd, J. Sun, D. Ouellette, K.L. Grant, X.C. Tang, M.J. Pikal, Mechanism of protein stabilization by sugars during freeze-drying and storage: native structure preservation, specific interaction, and/or immobilization in a glassy matrix?, J Pharm. Sci. 94 (2005) 1427–1444.
[39] B.S. Chang, G. Reeder, J.F. Carpenter, Development of a stable freeze-dried formulation of recombinant human interleukin-1 receptor antagonist, Pharm. Res. 13 (1996) 243–249.
[40] J.L. Cleland, X. Lam, B. Kendrick, J. Yang, T.H. Yang, D. Overcashier, D. Brooks, C. Hsu, J.F. Carpenter, A specific molar ratio of stabilizer to protein is required for storage stability of a lyophilized monoclonal antibody, J. Pharm. Sci. 90 (2001) 310–321.
[41] S.U. Sane, R. Wong, C.C. Hsu, Raman spectroscopic characterization of drying-induced structural changes in a therapeutic antibody: correlating structural changes with long-term stability, J. Pharm. Sci. 93 (2004) 1005–1018.
[42] J.D. Andya, C.C. Hsu, S.J. Shire, Mechanisms of aggregate formation and carbohydrate excipient stabilization of lyophilized humanized monoclonal antibody formulations, AAPS PharmSci 5 (2003) E10.
[43] K. Schersch, O. Betz, P. Garidel, S. Muehlau, S. Bassarab, G. Winter, Systematic investigation of the effect of lyophilizate collapse on pharmaceutically relevant proteins I: stability after freeze-drying, J. Pharm. Sci. 99 (2010) 2256–2278.
[44] E. Meister, H. Gieseler, Freeze-dry microscopy of protein/sugar mixtures: drying behavior, interpretation of collapse temperatures and a comparison to corresponding glass transition data, J. Pharm. Sci. 98 (2009) 3072–3087.
[45] K. Izutsu, K. Fujii, C. Katori, C. Yomota, T. Kawanishi, Y. Yoshihashi, E. Yonemochi, K. Terada, Effects of solute miscibility on the micro- and macroscopic structural integrity of freeze-dried solids, J. Pharm. Sci. 99 (2010) 4710–4719.

Biomaterials 35 (2014) 1347–1358

Contents lists available at ScienceDirect

Biomaterials

journal homepage: www.elsevier.com/locate/biomaterials

Leading opinion

Elucidating the molecular mechanism for the intracellular trafficking and fate of block copolymer micelles and their components

Kumiko Sakai-Kato [a,*], Keita Un [a], Kunie Nanjo [a], Nobuhiro Nishiyama [b], Hiroyuki Kusuhara [c], Kazunori Kataoka [d,e], Toru Kawanishi [f], Yukihiro Goda [a], Haruhiro Okuda [f]

[a] Division of Drugs, National Institute of Health Sciences, 1-18-1 Kamiyoga, Setagaya-ku, Tokyo 158-8501, Japan
[b] Polymer Chemistry Division, Chemical Resources Laboratory, Tokyo Institute of Technology, R1-11, 4259 Nagatsuda, Midori, Yokohama 226-8503, Japan
[c] Laboratory of Molecular Pharmacokinetics, Graduate School of Pharmaceutical Sciences, The University of Tokyo, 7-3-1 Hongo, Bunkyo, Tokyo 113-0033, Japan
[d] Center for Disease Biology and Integrative Medicine, Graduate School of Medicine, The University of Tokyo, 7-3-1 Hongo, Bunkyo, Tokyo 113-0033, Japan
[e] Department of Materials Engineering, Graduate School of Engineering, The University of Tokyo, 7-3-1 Hongo, Bunkyo, Tokyo 113-8656, Japan
[f] National Institute of Health Sciences, 1-18-1 Kamiyoga, Setagaya-ku, Tokyo 158-8501, Japan

ARTICLE INFO

Article history:
Received 17 October 2013
Accepted 8 November 2013
Available online 2 December 2013

Keywords:
Block copolymer micelles
Intracellular trafficking
Intermembrane transport
NPC1
ORP2
ABCB1

ABSTRACT

Block copolymer micelles have shown promise for the intracellular delivery of chemotherapeutic agents, proteins, and nucleic acids. Understanding the mechanism of their intracellular trafficking and fate, including the extracellular efflux of the polymers, will help improve their efficacy and minimize their safety risks. In this Leading Opinion paper, we discuss the molecular mechanism of block copolymer micelle trafficking, from intracellular uptake to extracellular efflux, on the basis of studies with HeLa cells. By using FRET (fluorescence resonance energy transfer) with confocal microscopy, we found that, following their intracellular transport via endocytosis, the micelles dissociated into their polymeric components in late endosomes and/or lysosomes. Furthermore, we confirmed that the intrinsic proteins NPC1 and ORP2 are involved in the intermembrane transfer of polymers from the endosome to the plasma membrane via the ER (endoplasmic reticulum) by using knockdown experiments with siRNAs. After the polymers were transported to the plasma membrane with the aid of ORP2, they were extruded into the cell medium via ABC transporter, ABCB1. Experiments with ABCB1-expressing vesicles indicated that the polymer itself, and not the fluorescent compounds, was recognized by the transporter. These findings, and the analysis of related mechanisms, provide valuable information that should help minimize the potential risks associated with the intracellular accumulation of block copolymer micelles and to improve their therapeutic efficacy.

1. Introduction

Drug delivery systems that use nanometer-sized carriers show promise for the targeted transfer of chemotherapeutic agents, proteins, and nucleic acids to tissues or organs. Nanomaterials have been extensively studied as drug carriers, and some formulations for cancer treatment have been applied clinically [1–3]. Block copolymer micelles have recently received considerable attention as targetable carrier systems [4–7]. The formulation of block copolymer micelles can alter the pharmacokinetic characteristics such as the volume of distribution, clearance, half-life, and tissue distribution of the active substances included [8–10]. Moreover, finely tuning the design of the block copolymers can increase their longevity in the bloodstream and allow the controlled release of the drugs, which consequently improves the pharmacodynamics of the drugs and/or avoids systemic toxicity.

The development of these drug carriers for the cellular uptake of therapeutic proteins and nucleic acids is of particular interest. Because nucleic acids, proteins, and peptides are not taken up into cells via passive diffusion, their intracellular uptake by nanocarriers is a key to targeting the delivery of these compounds at the cellular or organelle level. Specifically, the incorporation of these compounds into nanocarriers will improve the efficiency of their intracellular uptake or delivery to specific organelle, thereby ensuring their therapeutic effects. Furthermore, clarifying the intracellular trafficking mechanisms may also facilitate the

* Corresponding author. Tel./fax: +81 3 3700 9662.
E-mail address: kumikato@nihs.go.jp (K. Sakai-Kato).

0142-9612/$ – see front matter © 2013 Elsevier Ltd. All rights reserved.
http://dx.doi.org/10.1016/j.biomaterials.2013.11.027

discovery of new drug delivery strategies, such as targeting to specific cell organelles. Thus, to improve the efficiency of the intracellular uptake of these compounds, it is essential to understand the detailed mechanism of their trafficking including the fate of the micelles and their component polymers after their uptake via endocytosis. To this end, the use of covalently bound fluorescent reagents as probes has gradually shed light on the internalization pathways and intracellular localizations of polymeric nanoparticulate carriers [11–13].

In parallel, the safety of these carriers must be investigated. To ensure that these materials are safe, it is essential to know whether the components of the carriers are accumulated inside the cell or undergo sequestration (i.e., metabolism or efflux). The potential long-term effects of these novel polymers when used as nanosized particles have not yet been determined. To address this issue, we investigated the intracellular fate of polymer micelles conjugated with doxorubicin (Dox) in HeLa cells [14]. We demonstrated that Dox is endocytosed and localized to the endoplasmic reticulum, and that an ABC transporter, ABCB1, is involved in the efflux of the polymer from these cells. However, many factors remain unknown, for example, where do the micelles dissociate into their constituent polymers after internalization? What are the molecular mechanisms involved in trafficking to each organelle and in the efflux of polymers or micelles? Moreover, the trafficking phenomenon we found previously was limited to the case of Dox-conjugated polymers. Questions remain regarding the trafficking of other block copolymers, for example, those conjugated with different compounds or those with different poly(ethylene glycol) (PEG) lengths.

In the present study, we constructed three micelles by using three block copolymers (doxorubicin, Nile Red, and DBD (4-(*N*,*N*-dimethylsulfamoyl)-2,1,3-benzoxadiazole)) with different poly(ethylene glycol) (PEG) lengths (Mw 5000 or 12,000), detailed descriptions of which can be found in Section 3.1. To investigate the structural integrity of the micelles inside the cells, fluorescence resonance energy transfer (FRET) micelles were also constructed by using two types of polymers, that is, polymers with covalently bound Nile Red and polymers with covalently bound DBD. The trafficking of the micelles and their components, from intracellular uptake to extracellular efflux, was evaluated and the intrinsic molecules involved in the trafficking process were identified.

2. Materials and methods

2.1. Materials

Poly(ethylene glycol)–poly(aspartate) (PEG–P(Asp)) block copolymers with conjugated Dox were synthesized by Nippon Kayaku Co., Ltd. (Tokyo, Japan) [15]. Dextran (Dextran Texas Red, Molecular weight 10,000), polystyrene particles (FluoSphere Red, average particle size; 40.1 nm), Dulbecco's modified Eagle's Medium (DMEM), RPMI-1640, penicillin/streptomycin, and Opti-MEM I were purchased from Life Technologies (Brooklyn, NY, USA). Fetal bovine serum (FBS) was obtained from Nichirei Biosciences (Tokyo, Japan). Fluorescently labeled amorphous silica particles (Sicastar RedF, average particle size; 45.5 nm) were obtained from Micromod Partikeltechnologie (Rostock, Germany). Isolated mammalian cell membranes containing human ABCB1, for vesicle transport assays, (SB-MDR1-K-VT) were purchased from SOLVO Biotechnology (Hungary). All chemicals used in this study were of the highest purity available. HeLa cells (Health Science Research Resources Bank, Osaka, Japan) were cultured in DMEM. The medium was supplemented with 10% FBS, 100 U/mL penicillin/streptomycin. Cells were grown in a humidified incubator at 37 °C/5% CO_2.

2.2. Synthesis of the DBD-conjugated polymer and Nile Red-conjugated polymer

Poly(ethylene glycol)–poly(aspartate) block copolymer (PEG–P(Asp)) was obtained as described previously [15]. The degree of polymerization of PEG–P(Asp) was determined to be 35–45 by neutralization titration (Supplementary Fig. 1-1).

For the synthesis of DBD-conjugated polymer, PEG–P(Asp) (100 mg) and dimethylaminopyridine (23 mg, 0.8 equiv. for COOH) were dissolved in DMF (1.5 mL) and then DBD-ED (13 mg, 0.2 equiv.) and 4-phenyl-1-butanol (25 μL, 0.7 equiv.) were added. Diisopropylcarbodiimide (36 μL, 1.0 equiv.) was added to the solution and stirred at room temperature for 5 h. Diisopropylcarbodiimide (36 μL, 1.0 equiv.) was added again and the solution was stirred for 18 h. The reaction mixture was then dropped into a mixture of ethyl acetate and hexane (1:3). The resulting precipitate was filtered, washed with the mixture of ethyl acetate and hexane (1:3), and dried under vacuum to obtain the DBD-conjugated polymer (99 mg) as a powder. ^{1}H NMR spectra in DMSO-d_6 and the assignment are shown in Supplementary Fig. 1-2.

For the synthesis of the Nile Red-conjugated polymer, PEG–P(Asp) (100 mg) and dimethylaminopyridine (28 mg, 1.0 equiv.) were dissolved in DMF (1.5 mL) and then Nile-Red (8.8 mg, 0.1 equiv.) and 4-phenyl-1-butanol (36 μL, 1.0 equiv.) were added. Diisopropylcarbodiimide (36 μL, 1.0 equiv.) was added to the solution, which was then stirred at room temperature for 18 h. The reaction mixture was dropped into a mixture of ethyl acetate and hexane (1:3). The resulting precipitate was filtered, washed with the mixture of ethyl acetate and hexane (1:3), and dried under vacuum to obtain the Nile Red-conjugated polymer (109 mg) as a powder. ^{1}H NMR spectra in DMSO-d_6 and the assignment are shown in Supplementary Fig. 1-3.

2.3. Physicochemical properties of block copolymer micelles

The particle size and polydispersity index (PDI) of the block copolymer micelles were determined with a Zetasizer Nano ZS instrument (Malvern Instruments, Worcestershire, UK).

2.4. Evaluation of the intracellular trafficking of block copolymer micelles

To quantify the intracellular uptake of the polymers, we used a final polymer concentration of 50 μg/mL in this study. HeLa cells (5×10^4) were seeded onto 6-well plates in medium containing 10% FBS and 100 U/mL penicillin/streptomycin. After incubation for 24 h at 37 °C/5% CO_2, the cells were exposed to 50 μg/mL micelles in culture medium. After incubation for pre-determined durations, the incubation medium was replaced with Hanks' balanced salt solution (HBSS). The cells were trypsinized with 0.25% trypsin–ethylenediamine tetraacetic acid (EDTA) (Life Technologies), washed with HBSS three times, and suspended in lysis buffer (1.0% Triton X-100 in HBSS). The cell suspension was then shaken and centrifuged (15,000× *g*, 4 °C, 10 min). The fluorescence intensity of the resultant supernatant was measured on a fluorescence spectrophotometer (F-7000; Hitachi High-Technologies, Tokyo, Japan) using 440 nm excitation and 580 nm emission for DBD-conjugated polymers, 580 nm excitation and 640 nm emission for Nile Red-conjugated polymers, and 470 nm excitation and 590 nm emission for Dox-conjugated polymers. The fluorescence intensity was normalized with respect to the protein content of the cells. The protein concentration was determined by using a Protein Assay Kit (Bio-Rad Laboratories, Hercules, CA, USA).

2.5. Confocal microscopy

To observe the colocalization of block copolymer micelles with the intracellular compartment, specific intracellular compartment components were labeled by using fluorescent dyes. All dyes for confocal microscopy were purchased from Life Technologies and used in accordance with the manufacturer's instructions. Endosomes were labeled with transferrin conjugated to Alexa Fluor 488 or Alexa Fluor 594, and lysosomes were labeled with LysoTracker Green DND-26 or LysoTracker Red DND-99. The ER was labeled with ER-Tracker Green or ER-Tracker Red, and the Golgi apparatus was labeled with Bodipy-FL C5-ceramide or Bodipy-TR C5-ceramide complexed to BSA. Confocal microscopy was performed as previously described [14]. Briefly, cells (1.0×10^5) were plated on 35-mm glass-bottom dishes coated with poly-L-lysine (Matsunami Glass, Osaka, Japan) in medium containing 10% FBS and 100 U/mL penicillin/streptomycin. After incubation for 24 h, cells were exposed to 50 μg/mL micelles in culture medium. At a pre-determined time after addition of the micelles, cells were washed and kept in HBSS for imaging with a confocal microscope (Carl Zeiss LSM 510; Carl Zeiss Microscopy GmbH, Germany). Pseudocolor luminescent images were captured using LSM Image Browser (Carl Zeiss Microscopy GmbH, Germany).

An FRET experiment was performed using FRET micelles composed of DBD-conjugated polymers and Nile Red polymers (9:1, w:w). Cells were exposed to 50 μg/mL FRET micelles in culture medium. Two hours after addition of the micelles, cells were washed and kept in medium without micelles and then imaged with a confocal microscope at 2, 10, and 24 h after addition of the micelles.

2.6. Endocytosis inhibition and Golgi destruction

To investigate the mechanism of endocytosis of the prepared micelles, 10 μg/mL chlorpromazine (a clathrin-mediated endocytosis inhibitor), 150 μM genistein or 2.0 mM methyl-β-cyclodextrin (MβCD) (caveolae-mediated endocytosis inhibitors), or 50 μM 5-(N-ethyl-N-isopropyl) amiloride (a macropinocytosis inhibitor) were used [16,17]. Each endocytosis inhibitor was added to the culture medium 30 min before the addition of the micelles. To inhibit ER-to-Golgi transfer, to investigate whether ER-to-Golgi transfer is involved in the intracellular trafficking of micelles or polymers, cells were incubated in medium containing 1 μg/mL brefeldin A 30 min before the addition of the micelles [18].

2.7. Small interfering RNA (siRNA) transfer

To clarify which intrinsic proteins are involved in the intracellular trafficking and efflux of the polymers, the expression of specific proteins was down-regulated by

using siRNA. Stealth RNAi oligonucleotides (25-mer, Life Technologies), which unlike conventional siRNAs can reduce the cytotoxic interferon response [19], were obtained from Life Technologies. The siRNA sequences used in this study are shown in Table 1. As a negative control, the Stealth RNAi High GC Negative Control Duplex (Life Technologies) was used [14]. The Stealth RNAi oligonucleotides were transfected into cells by using Lipofectamine RNAiMAX (Life Technologies) according to the manufacturer's protocols. Briefly, the cells were incubated for 24 h. Each siRNA was then added, and the cells were incubated for a further 48 h, at which time the micelles (50 μg/mL) were added. Western blotting was used to confirm the down-regulation of each protein as described previously [14]. After the cells were incubated with the micelles, the culture medium was replaced with HBSS. Cells were trypsinized and lysed to quantify the intracellular amount of polymer as described above (Section 2.3).

2.8. Transport experiment

To investigate ATP-dependent transport, mammalian cell membrane vesicles expressing ABCB1 were used according to the manufacturer's instructions. Suspensions of vesicles expressing ABCB1, and control vesicles without ABCB1 (50 μL each), were plated on a 96-well plate. Samples (0.75 μL) at the indicated concentration and reaction buffer (25 μL) were added to each well, and the plates were incubated at 37 °C for 5 min. After washing by centrifugation (1500× g, 5 min, 4 °C), the fluorescence intensity of the polymers after intravesicular transport was measured using a fluorescence spectrophotometer as described in Section 2.3. The fluorescence intensity of intravesicular polymers incubated with MgATP was subtracted from that of polymers incubated without MgATP.

2.9. Statistical analyses

Results are presented as the mean ± SD of more than three experiments. Analysis of variance was used to test the statistical significance of the differences among groups. Two-group comparisons were performed with a Student's *t*-test. Multiple comparisons between control and test groups were performed with a Dunnett's test.

3. Results

3.1. Chemical structures of block copolymers and physicochemical properties

We used three different kinds of micelles formed from Dox-conjugated, DBD-conjugated, and Nile Red-conjugated PEG–P(Asp) block copolymers, respectively (Supplementary Fig. 1), hereinafter referred to as Dox-conjugated polymers, DBD-conjugated polymers, and Nile Red-conjugated polymers, respectively. Dox-conjugated polymers consisted of PEG (M_w ~5000) and P(Asp) (polymerization degree, 30) with partially conjugated doxorubicin (ca. 45%) to the side chain of the P(Asp) [15]. DBD-conjugated polymers consist of PEG (M_w ~12,000) and P(Asp) (polymerization degree, 35–45), with partially conjugated DBD (ca. 10%) and 4-phenyl-1-butanol (ca. 43%) to increase the hydrophobicity to the side chain of the P(Asp). Nile Red-conjugated polymers consist of PEG (M_w ~12,000) and P(Asp) (polymerization degree, 35–45) with partially conjugated Nile Red (ca. 10%) and 4-phenyl-1-butanol (ca. 53%) to increase the hydrophobicity to the side chain of the P(Asp). When these block copolymers were dissolved in aqueous medium, they spontaneously formed micelles with hydrophobic cores. We constructed FRET micelles by mixing DBD-conjugated polymers with Nile Red-conjugated polymers. The particle sizes of the resultant micelles (~30 nm) are shown in Table 2.

Table 2
Particle sizes and PDI of block copolymer micelles used in this study.

	Particle size	PDI
DBD-conjugated polymer micelles	31.7 ± 0.11	0.180 ± 0.011
NR-conjugated polymer micelles	31.4 ± 0.67	0.184 ± 0.006
Dox-conjugated polymer micelles	32.3 ± 0.19	0.180 ± 0.014
DBD:NR (9:1)-conjugated polymer micelles	32.4 ± 0.18	0.198 ± 0.005

Each value represents the mean ± S.D. ($n = 3$).

3.2. Endocytosis of block copolymers

To investigate the intracellular transport mechanisms of the micelles and their components, we used confocal microscopy to observe the intracellular trafficking of fluorescent micelles composed of Dox-, Nile Red- or DBD-conjugated polymers. All three of the different types of fluorescent micelle colocalized with the endosomes after 1 h in HeLa cells (Fig. 1A). At 2 h-post-incubation, most of the micelles colocalized with the lysosomes although some were distributed outside the vesicles (Fig. 1B).

The use of endocytosis inhibitors to clarify the endocytosis mechanism demonstrated that the internalized amounts of fluorescent micelles in HeLa cells were significantly suppressed at 2, 24 and 48 h in the presence of chlorpromazine (Fig. 2). Genistein and MβCD also inhibited the intracellular uptake of all of the micelles at 24 and 48 h, although the extent of inhibition was less in the case of genistein and MβCD compared with that of chlorpromazine. These results indicate that the intracellular uptake of the micelles proceeded mainly through clathrin-mediated endocytosis. Caveolae-mediated endocytosis also contributed to the uptake over time.

3.3. Dissociation of micelles into polymers in HeLa cells

We then attempted to identify the intracellular location where the block copolymer micelles dissociate into polymers after internalization. We constructed an FRET system to track the structural integrity of the micelles once they were internalized into the HeLa cells. FRET is a distance-dependent process in which excitation energy is absorbed by a molecular fluorophore (the donor) and then transferred to a nearby fluorophore (the acceptor). It is a highly sensitive technique for investigating biological phenomena that produce changes in molecular proximity [20,21]. We used micelles consisting of DBD-conjugated polymers and Nile Red-conjugated polymers (9:1, w/w; Fig. 3A). The mixing ratio of 9:1 of DBD-:Nile Red-conjugated polymers resulted in the formation of

Table 1
The siRNA sequences used in this study.

Target gene	Sense strand	Antisense strand
MLN64	5′-GCUGA AGGAU UAAAC AAUGA CUUCA-3′	5′-UGAAG UCAUU GUUUA AUCCU UCAGC-3′
ORP1	5′-GCACC UCUGA GGAGU UGGAU GAAAU-3′	5′-AUUUC AUCCA ACUCC UCAGA GGUGC-3′
NPC1	5′-CCCUC GUCCU GGAUC GACGA UUAUU-3′	5′-AAUAA UCGUC GAUCC AGGAC GAGGG-3′
CERT	5′-ACGUG AGAAG UUGGC UGAAA UGGAA-3′	5′-UUCCA UUUCA GCCAA CUUCU CACGU-3′
Sec31A	5′-CCAGG CCAAU AAGCU GGGUG UCUAA-3′	5′-UUAGA CACCC AGCUU AUUGG CCUGG-3′
ORP2	5′-GAGAG GAGAG GUGAC CACCU GAGAA-3′	5′-UUCUC AGGUG GUCAC CUCUC CUCUC-3′
PITP	5′-GGAUA UUUAC AAACU UCCAU CGCCA-3′	5′-UGGCG AUGGA AGUUU GUAAA UAUCC-3′
ABCA1	5′-UUUAG AUGCU GGACA CUGCC AAGGC-3′	5′-GCCUU GGCAG UGUCC AGCAU CUAAA-3′
ABCB1	5′-UCCCG UAGAA ACCUU ACAUU UAUGG-3′	5′-CCAUA AAUGU AAGGU UUCUA CGGGA-3′
ABCC1	5′-CCGGU CUAUU CCCAU UUCAA CGAGA-3′	5′-UCUCG UUGAA AUGGG AAUAG ACCGG-3′
ABCG1	5′-UCUCG CUGAU GAAAG GGCUC GCUCA-3′	5′-UGAGC GAGCC CUUUC AUCAG CGAGA-3′
Snap-25	5′-CAUGG AGAAG GCUGA UUCCA ACAAA-3′	5′-UUUGU UGGAA UCAGC CUUCU CCAUG-3′

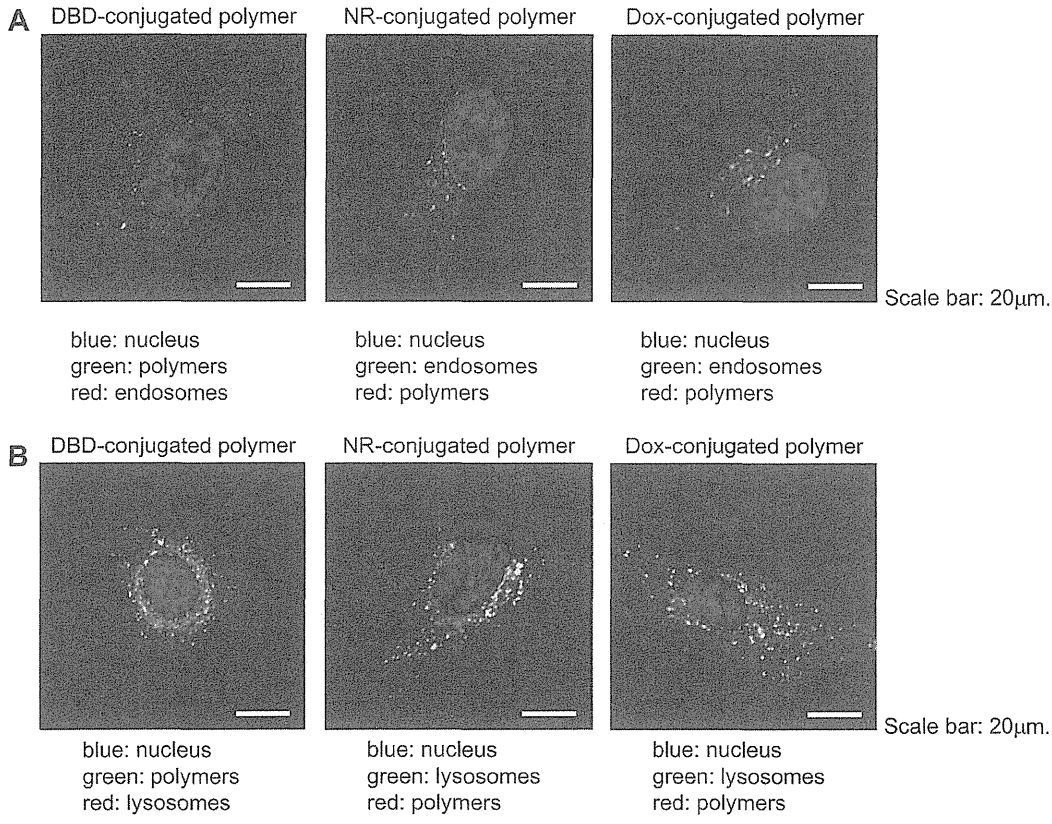

Fig. 1. (A) Confocal images showing the intracellular transport of micelles at 1 h after the addition of the micelles to HeLa cells. The endosomes are labeled with Alexa Fluor-conjugated transferrin. Scale bars = 20 μm. (B) Confocal images showing the intracellular transport of micelles at 2 h after the addition of the micelles to HeLa cells. The lysosomes are labeled with LysoTracker Red or Green. Scale bars = 20 μm.

block copolymer micelles with the most effective FRET efficiency. At 2 h after the addition of the micelles, we washed the cells with fresh medium to stop any further entry of micelles into the HeLa cells, whereupon only red (in web version) fluorescence was observed in the vesicular structure (Fig. 3B). Together with the result of the cellular uptake experiments, these results show that the block copolymers mostly maintain their micellar structure for at least 2 h after their internalization. Confocal microscopy images were taken at time intervals up to 24 h after the addition of the micelles. The fluorescence of the vesicular structures changed to yellow (in web version) after 10 h and then to green (in web version) after 24 h suggesting that the micelles gradually dissociated into polymers upon localization in the endosomes and/or lysosomes (Fig. 3B).

3.4. Intracellular trafficking of block copolymers

Using confocal microscopy, we further examined the intracellular trafficking of block copolymers with conjugated fluorescent compounds after their internalization. The fluorescence of all three polymers was colocalized to the ER, but not to the Golgi apparatus of the HeLa cells (Fig. 4). This is consistent with our previous study showing that Dox-bound micelles colocalize to the ER but not to the Golgi apparatus [14].

3.5. Molecular mechanisms of intracellular trafficking from endosomes/lysosomes to the cytoplasm and ER

In the case of cholesterol, there is some evidence for a direct pathway from endosomes to the ER [22,23]. We, therefore, investigated whether the molecular mechanisms involved in the transport of cholesterol or other lipid analogs are also implicated in the intracellular trafficking of block copolymers. To elucidate the molecular mechanisms of block copolymer transport in HeLa cells, we used siRNAs to down-regulate the expression of specific lipid transport proteins. We hypothesized that the suppression of specific intracellular transport processes would decrease the extracellular efflux of the block copolymers, thereby leading to an increase in the intracellular amounts of each polymer. Fig. 5A shows the intracellular components and the typical lipid transport proteins we investigated. At 48 h after transfection with stealth RNAis, the expression of each protein was down-regulated in HeLa cells, which allowed us to investigate the role of these proteins in polymer transport (Supplementary Fig. 2). Initially, we investigated lipid transport proteins that are involved in intracellular trafficking from endosomes/lysosomes to other compartments, including the ER. These proteins included metastatic lymph-node gene 64 protein (MLN64) [24], oxysterol-binding protein-related protein 1 (ORP1) [25], and Niemann–Pick C1 protein (NPC1) [26,27]. Fig. 5B shows the amounts of intracellular polymer increased upon suppression of NPC1 expression. Confocal microscopy also revealed that the transport of polymers from endosomes or lysosomes to the ER was suppressed when NPC1 expression was knocked-down (Fig. 5C). These results suggest that NPC1 partially controls the intracellular trafficking of the polymers from the endosomes or lysosomes to the ER. On the other hand, they also indicate that MLN64 and ORP1, which are sterol-binding proteins that are involved in organizing late endosomal membrane trafficking, are not involved in the trafficking of these polymers. To determine

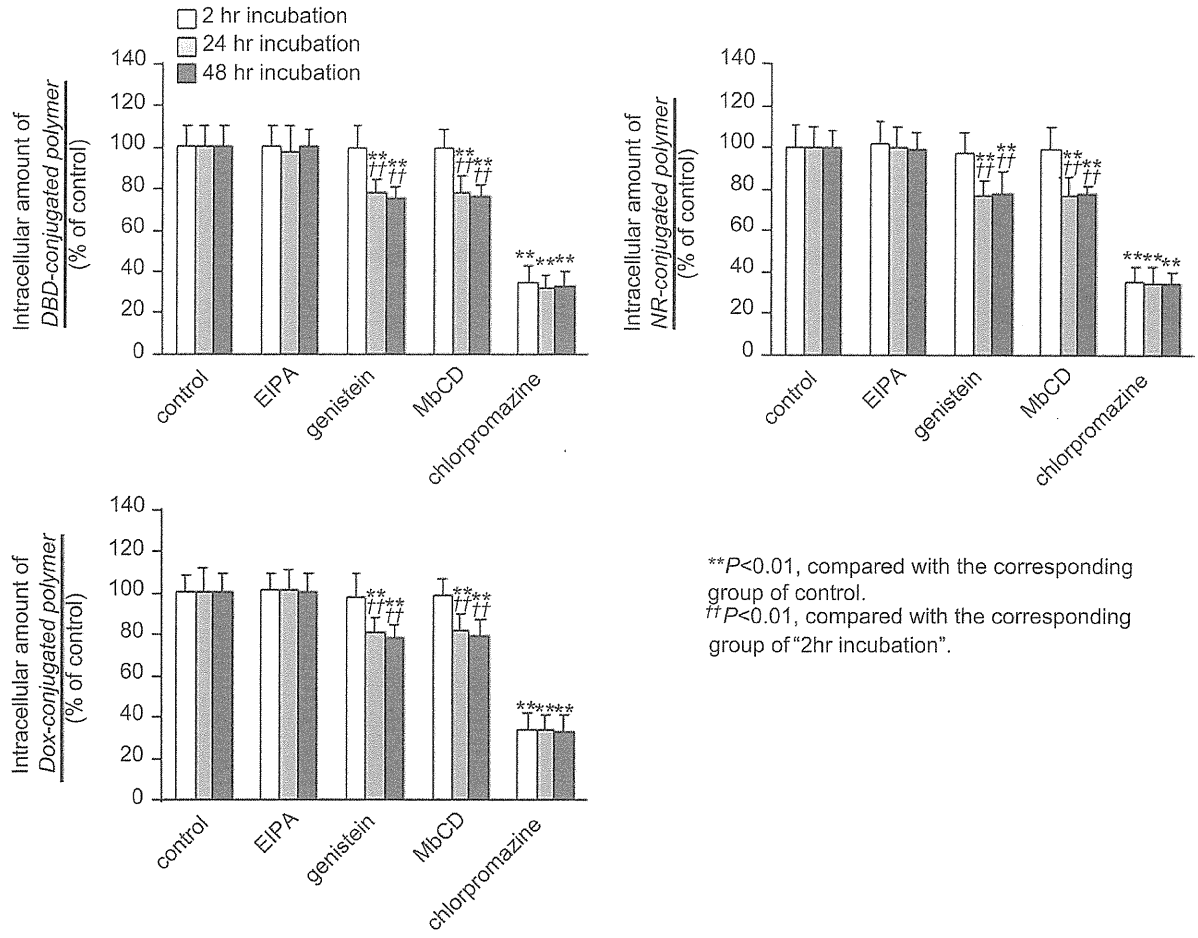

Fig. 2. The effect of endocytosis inhibitors on the intracellular amounts of polymers. The intracellular transport of micelles was evaluated at 2, 24, and 48 h after the addition of micelles to HeLa cells. Each endocytosis inhibitor was added to the cells 30 min before the addition of the micelles. $^{**}P < 0.01$ compared with the corresponding control group. $^{††}P < 0.01$, compared with the corresponding group of "cells incubated for 2 h". Each value represents the mean ± SD ($n = 6$).

whether the absence of NPC1 also leads to increased retention of other polymers or nanoparticles that are internalized via endocytosis, we tested dextran, polystyrene nanoparticle, and silica nanoparticle. We found that the amounts of intracellular dextran, polystyrene nanoparticles, and silica nanoparticles were not affected by the suppression of NPC1 expression (Supplementary Fig. 3). These results thus show that NPC1 is not involved in trafficking of all polymers or nanoparticles from NPC1-positive late endosomes.

ER-to-Golgi transport is a major trafficking route for lipid molecules. Therefore, we investigated the involvement of ER-to-Golgi transport in the intracellular trafficking of block copolymers by examining whether trafficking was affected if ER-to-Golgi transport-related proteins were inhibited. We selected CERT, a known ceramide-transfer protein [28,29], and sec31A, a component of COPII that is required for the budding of vesicles from the ER [30,31] (Fig. 5A) for this assessment. The intracellular amounts of polymer were not affected by CERT or sec31A knockdown (Supplementary Fig. 4A), nor were they affected by the presence of brefeldin A, an inhibitor of the transport pathway from the ER to the Golgi apparatus [18] (Supplementary Fig. 4B). These results suggest that the ER-to-Golgi transport system is not involved in polymer trafficking, which is consistent with our results indicating that the polymers did not localize to the Golgi apparatus (Fig. 4B).

3.6. Molecular mechanism for the extracellular efflux of polymers

To investigate the transport of polymers to the plasma membrane, we examined oxysterol-binding protein-related protein 2 (ORP2) [32–34] and phosphatidylinositol transfer protein (PITP) [35–37]. These proteins are both involved in the intracellular transport of lipid molecules (Fig. 5A). Knockdown experiments using siRNAs against each protein revealed that the intracellular amounts of all three polymers did not change with the suppression of PITP, but increased upon the suppression of ORP2, a molecule involved in the trafficking of endogenous cholesterol (Fig. 6). On the other hand, the intracellular amounts of dextran, silica nanoparticles, and polystyrene nanoparticles were not affected by the suppression of ORP2 expression. (Supplementary Fig. 5A).

We previously reported that ABCB1, a member of the ATP-binding cassette (ABC) transporter family, is involved in the efflux of Dox-conjugated block copolymers [14]. ABCB1, also known as MDR-1 or P-gp, is an efflux pump for various drugs. In this study, we assessed the involvement of other types of ABC transporters and exocytosis in the extracellular efflux of polymers from HeLa cells. The knockdown of various ABC transporters (ABCA1, ABCB1, ABCC1, and ABCG1) caused the intracellular amounts of all polymers at 24 h after micelle addition to increase when ABCB1 expression was suppressed, but not when ABCA1, ABCC1, or ABCG1 expression was

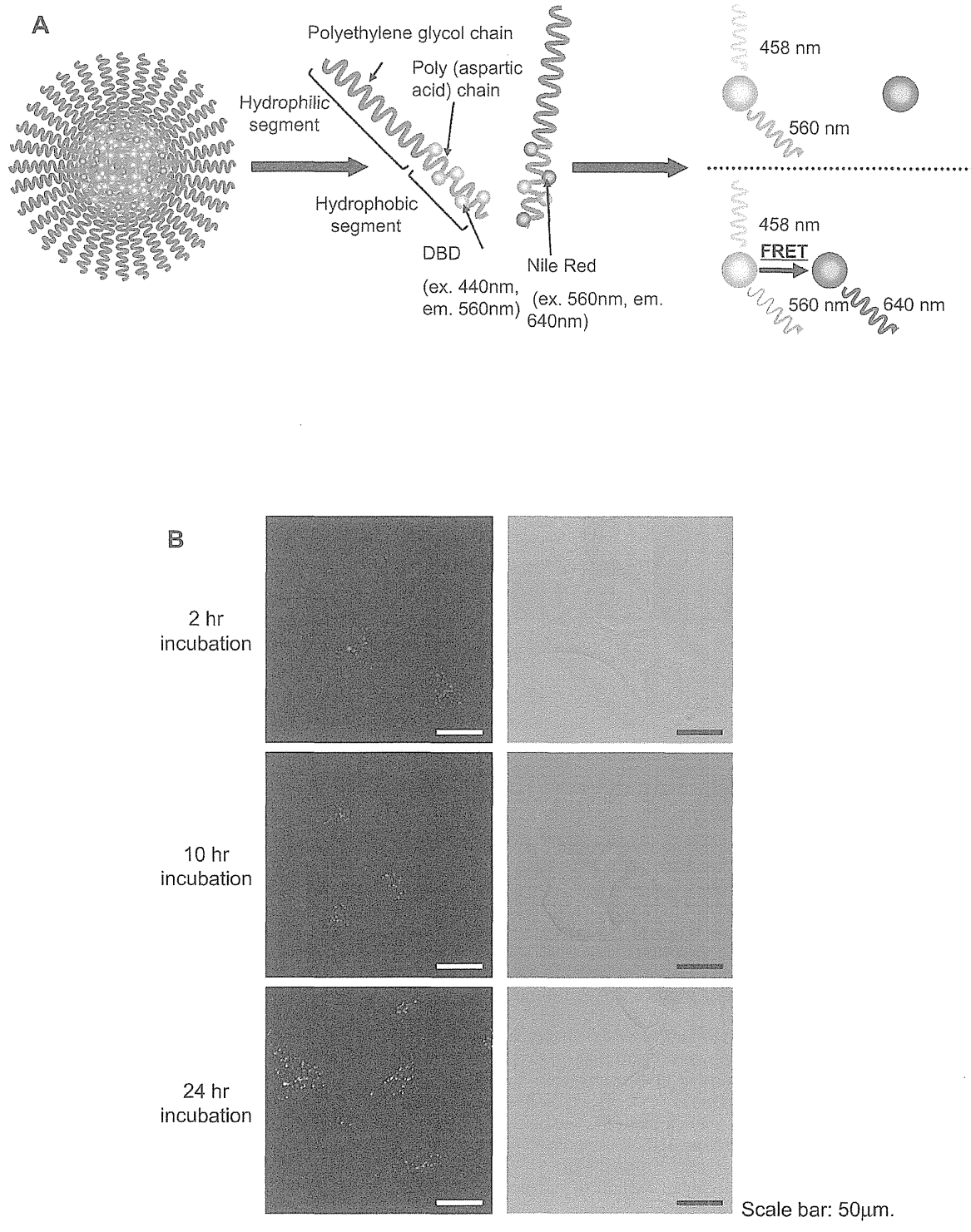

Fig. 3. (A) Schematic of FRET micelles used to investigate the structural integrity of micelles in HeLa cells. The fluorescent intensity of the donor, DBD (excitation 440 nm; emission 580 nm), enhanced the effective excitation of the acceptor, Nile Red (excitation 580 nm; emission 640 nm). (B) Confocal images of the fluorescent spectral shift that corresponds to the dissociation of FRET micelles. Cells were exposed to 50 μg/mL FRET micelles in culture medium. Two hours after the addition of micelles, the cells were washed and kept in medium without micelles; they were then subjected to confocal imaging at 2, 10, and 24 h after the addition of the micelles. Scale bars = 50 μm.

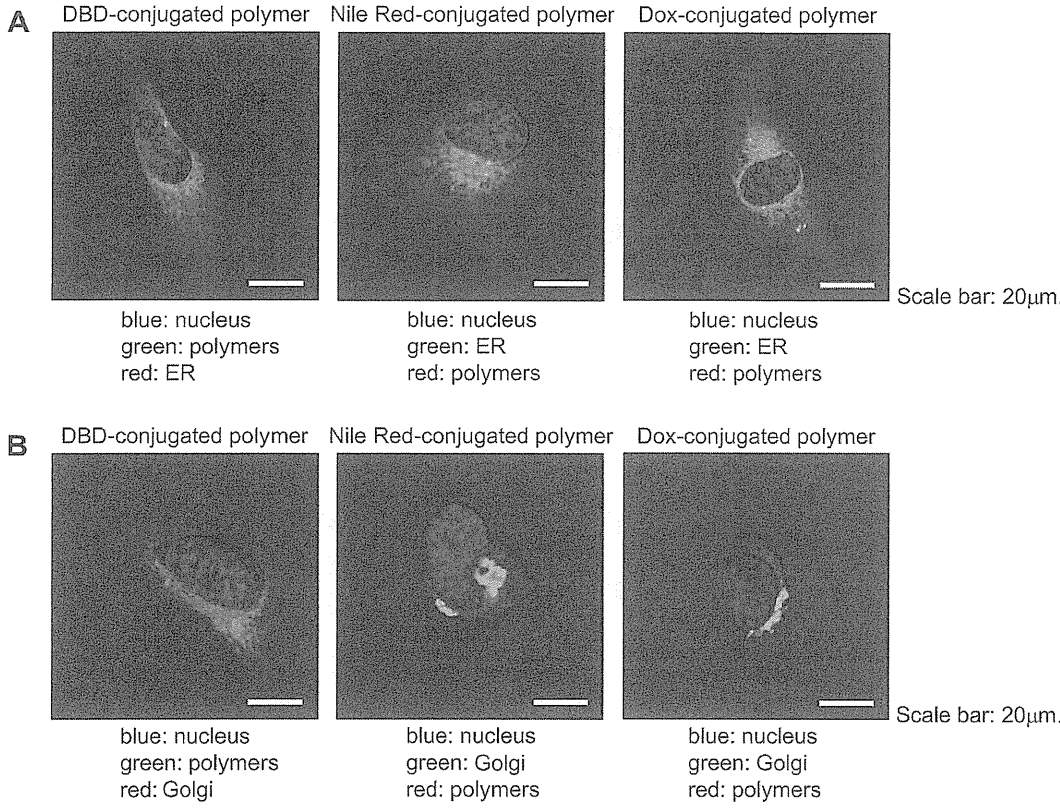

Fig. 4. Confocal images showing the intracellular localization of polymers at 24 h after the addition of micelles to HeLa cells. ER (A) and Golgi apparatus (B) were labeled with ER-Tracker and BODIPY-ceramide, respectively. Scale bars = 20 μm.

suppressed (Fig. 7A). On the other hand, the suppression of ABCB1 transporter expression did not lead to an increase in the intracellular amounts of dextran, polystyrene nanoparticle, or silica nanoparticle (Supplementary Fig. 5B).

With respect to exocytosis, the intracellular amounts of the polymers were also unaffected by the presence of snap-25, a known exocytosis-related protein (Fig. 7B).

3.7. The transport of polymers by ABCB1

The possibility remained that efflux only occurred for fluorescent compounds that were no longer conjugated to the polymers. Therefore, to further confirm the involvement of the ABCB1 transporter in the efflux of block copolymers, we used membranes expressing ABCB1. ATP-dependent transport increased at higher polymer concentrations for DBD-, Nile Red-, and Dox-conjugated polymers (Fig. 8A). All of the block polymers were transported through the membranes that expressed ABCB1, but were not transported through control membranes that lacked ABCB1 (Fig. 8B). To examine whether ABCB1 recognizes the conjugated fluorescent compounds or the polymer itself, we also examined the ATP-dependent transport of free DBD, Nile Red, and Dox and found that intravesicular uptake of DBD and Nile Red did not occur (Fig. 8C). Transport was observed for Dox, which is a well-known substrate of ABCB1. These findings indicate that the intravesicular fluorescence observed in our study and extracellular efflux observed in Fig. 7A did not stem from free fluorescent compounds, but rather from the fluorescent compounds conjugated to the polymers. Therefore, ABCB1 recognizes the block copolymer.

4. Discussion

The aim of this study was to elucidate the molecular mechanisms involved in the intracellular trafficking and extracellular efflux of block copolymer micelles and their components. In this study, we used block copolymer micelles conjugated with the fluorescent compounds Dox, DBD, and Nile Red.

The intracellular uptake of micelles was inhibited in the presence of chlorpromazine in HeLa cells (Fig. 2), suggesting that all micelles are taken up into the cells via clathrin-mediated endocytosis. However, caveolae-mediated endocytosis was also observed to some extent in all micelles as the incubation time progressed. The P85 amphiphilic triblock copolymer, which is composed of poly(ethylene oxide) (PEO) and poly(propylene oxide) (PPO), is internalized predominantly through caveolae-mediated endocytosis, although in the micelle form P85 is internalized exclusively through clathrin-mediated endocytosis [12,38].

FRET is a technique that has been used recently to measure the stability and dissociation of drug delivery system carriers and the release of encapsulated drugs. By using FRET micelles, we determined that micelle dissociation occurs within endosomes or lysosomes after internalization via endocytosis. This result indicates that the release of encapsulated drugs from these micelles will occur in endosomes or lysosomes.

We also investigated the molecular mechanisms involved in the intracellular trafficking of the block copolymers. When NPC1 expression was inhibited, the intracellular amounts of polymer increased (Fig. 5B). Confocal microscopy revealed that the knockdown of NPC1 expression suppressed the transport of the polymers

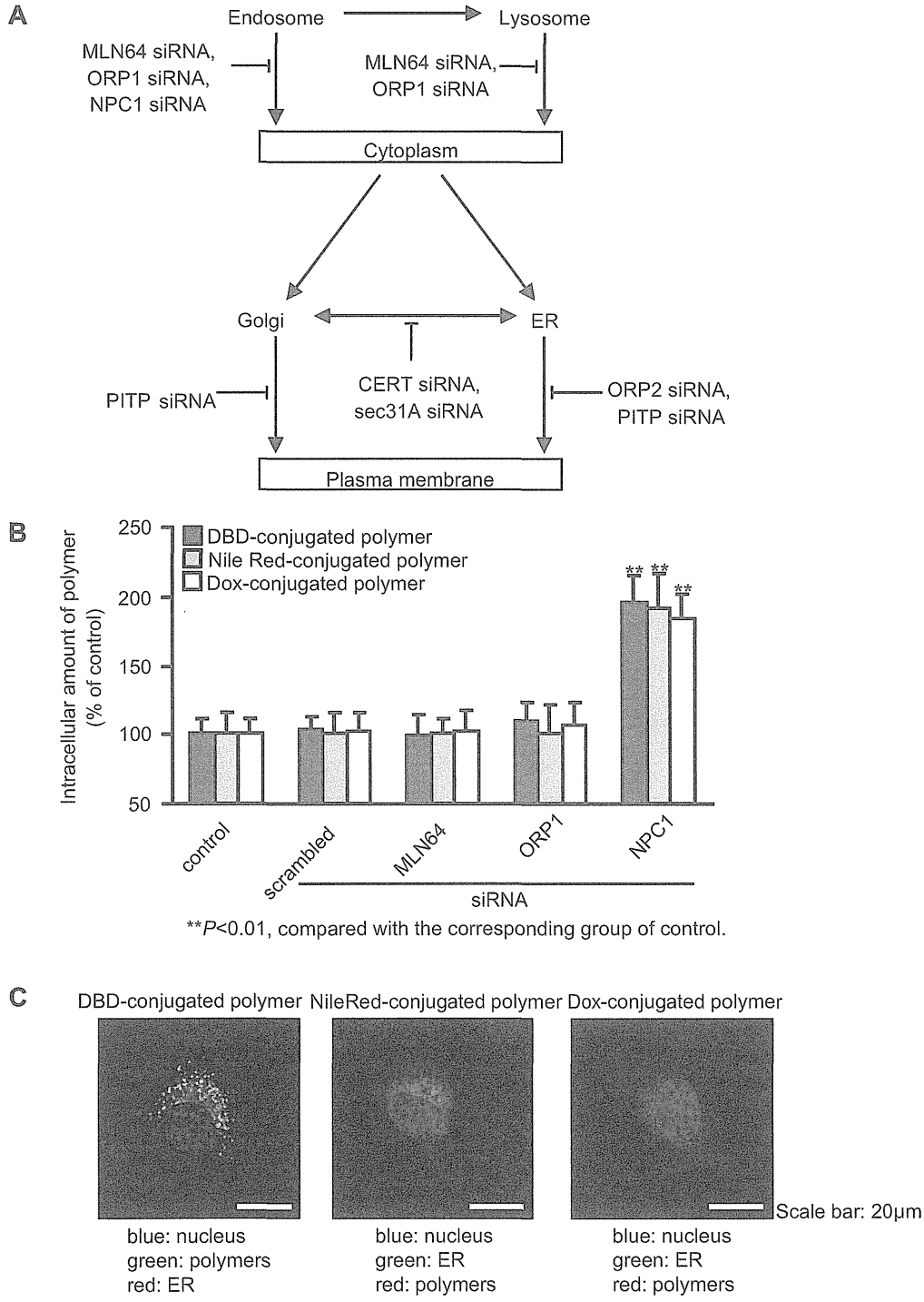

Fig. 5. (A) Intracellular components and typical lipid transport proteins. The expression of these proteins was suppressed by siRNA. (B) Intracellular amounts of polymers under suppressing conditions for each protein (MLN64, ORP1, and NPC1) at 24 h after the addition of micelles to HeLa cells. Cells were transfected with siRNAs against the targeted proteins by using Lipofectamine RNAiMAX according to the recommended protocols. $^{**}P < 0.01$ compared with the corresponding control group. Each value represents the mean ± SD ($n = 6$). (C) Confocal images showing the intracellular localization of micelles under suppressing conditions for NPC1 at 24 h after the addition of micelles to HeLa cells. The ER was labeled with ER-Tracker. Scale bars = 20 μm.

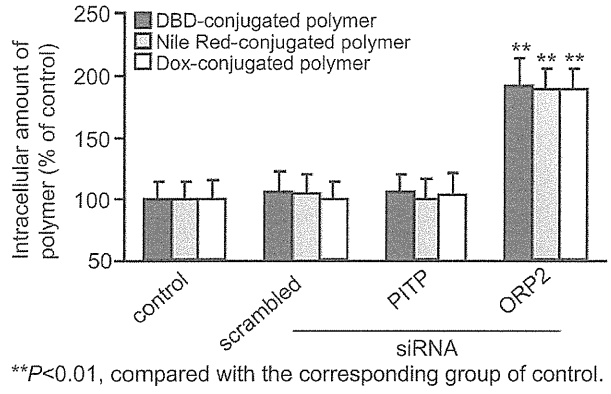

Fig. 6. Effect of siRNA-induced knockdown of ORP2 and PITP on the intracellular amounts of polymers. The figure shows the intracellular amounts of polymer under suppressing conditions for ORP2 or PITP at 24 h after the addition of micelles to HeLa cells. $^{**}P < 0.01$ compared with the corresponding control group. Each value represents the mean ± SD ($n = 6$).

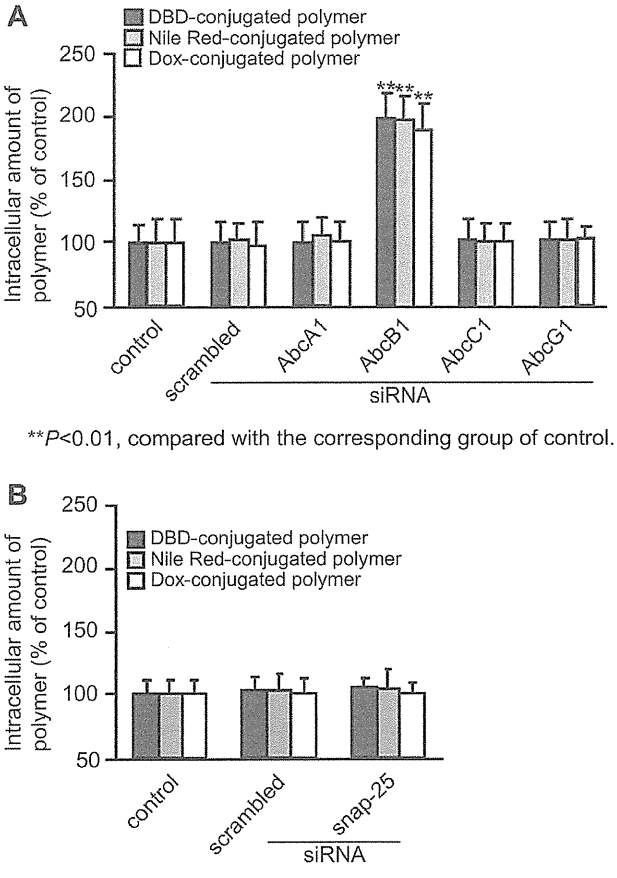

Fig. 7. (A) Effect of siRNA-induced knockdown of ABC transporters on the intracellular amounts of polymers. The figure shows the intracellular amounts of polymer under suppressing conditions for various ABC transporters (ABCA1, ABCB1, ABCC1, and ABCG1) at 24 h after the addition of micelles to HeLa cells. (B) The intracellular amounts of polymers under suppressing conditions for snap-25 at 24 h after the addition of micelles to HeLa cells. The cells were transfected with siRNAs against the targeted proteins by using Lipofectamine RNAiMAX according to the recommended protocols. $^{**}P < 0.01$ compared with the corresponding control group. Each value represents the mean ± SD ($n = 6$).

from endosomes or lysosomes to the ER (Fig. 5C). Our results also suggest that ER-to-Golgi transport is not involved in the intracellular trafficking of block copolymers (Supplementary Fig. 4). This is consistent with our observation that the polymer did not localize to the Golgi apparatus (Fig. 4B). Taken with the results of the FRET micelle experiments, the confocal images suggest that the micelles used in this study dissociate into their individual components in late endosomes, and after dissociation, the polymers are extracted by NPC1 from the endosomes and transferred to the ER (Fig. 9). We confirmed that 4-phenyl-1-butanol, which was conjugated to the polymers to increase their hydrophobicity, was not released from the polymers under the experimental conditions used (Supplementary Fig. 6). Therefore, the release of the conjugated compounds is not the driving force for the dissociation of the micelles in late endosomes or lysosomes. The driving force for this dissociation remains to be elucidated.

NPC1 facilitates the trafficking of low density lipoprotein-derived cholesterol from the late endosome to various destinations such as the plasma membrane, the trans-golgi network, and the ER [39]. Similarly, it appears that NPC1 enhances the trafficking of dissociated polymers from late endosomes to the ER. Although direct trafficking from the late endosome to the plasma membrane is a possibility [40], such trafficking would probably represent a small proportion of the total trafficking given our finding that the inhibition of trafficking from the ER to the plasma membrane led to the retention of most of the intracellular block copolymers. Sahay G et al. reported that NCP1 is an important regulator of the major recycling pathways of lipid nanoparticle-delivered siRNA, although they did not investigate the trafficking of the carrier components, but rather tracked the labeled siRNA. They demonstrated that NPC1-deficient cells show enhanced cellular retention of lipid nanoparticles inside late endosomes because of the decrease in motility of late endosomes [40,41]. These findings indicate that NPC1 is a key factor in determining the fate of block copolymers.

Although some of the block copolymers might have been retained in vesicles and transferred to lysosomes, the dissociated polymers in the late endosomes were transported to the ER. Our results also indicate that encapsulated drugs could be released from these micellar carriers in late endosomes and diffuse into the cytoplasm at this stage, demonstrating that such micelles are suitable for the intracellular delivery of degradable compounds, such as nucleic acids or proteins, and can minimize the degradation of these compounds in lysosomes. We also investigated the extracellular efflux mechanisms of block copolymers. As shown in Fig. 6, the transport of block copolymers to the cell membrane was affected by ORP2 (Fig. 9). ORP2 is involved in the vesicle-independent intermembrane transport of lipophilic compounds [32–34], and the ER possesses closed sites at the cell membrane [42]. Hao et al. reported that endogenous cholesterol is transported to cell membranes via the ER [43]. Therefore, the block copolymers in the present study might also be transferred to the cell membrane via these closed sites (Fig. 9). Following the transfer to the plasma membrane, efflux of the block copolymers mainly occurred via ABCB1 but not ABCA1, ABCC1, or ABCG1 (Figs. 7 and 9). SNARE proteins, such as snap-25, control the extracellular efflux of various compounds, including proteins and lipids, via exocytosis [44,45]. Although the expression levels of SNARE-related proteins are high in specific cancer cells, including HeLa cells [44–46], exocytosis did not appear to be involved in the extracellular efflux of block copolymers from HeLa cells (Fig. 7B), and the block copolymers used in our studies were effluxed only through the ABCB1.

Lastly, we investigated the molecular mechanism of block copolymer efflux through transporters by using vesicles that expressed ABCB1. All of the polymers, regardless of PEG chain length, polymerization degree of P(Asp), or fluorescent compound,

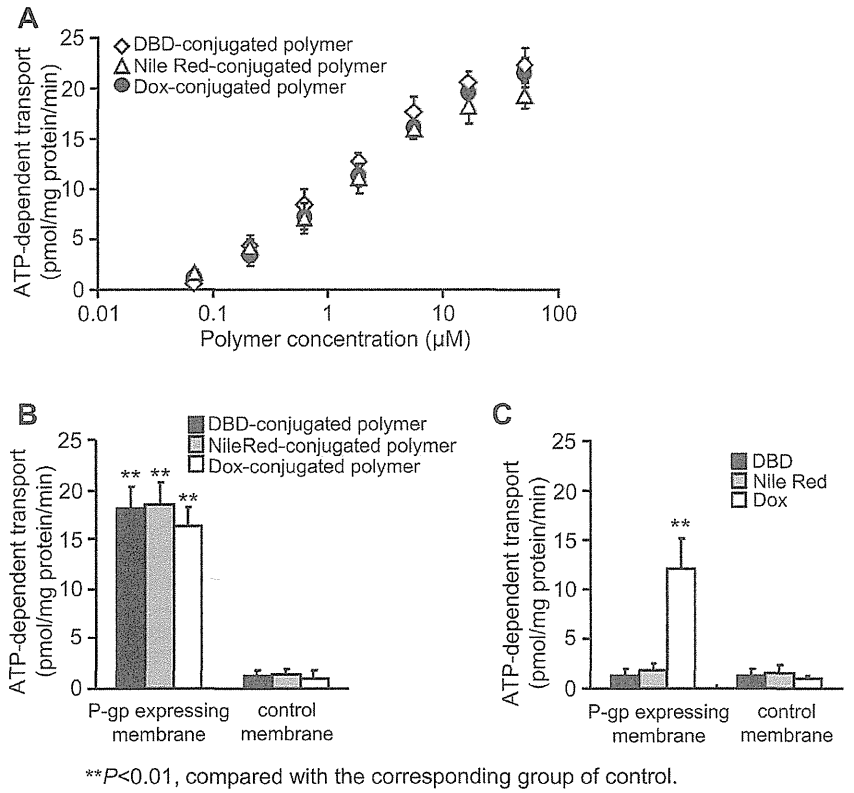

Fig. 8. ATP-dependent uptake of polymers by ABCB1-expressing membrane vesicles. Suspensions of membranes expressing ABCB1, or control membranes that did not express ABCB1 (50 μL each) were plated on a 96-well plate. (A) Increasing polymer transport with increasing polymer concentration. Samples at the indicated concentration were added to each well, respectively, and the plates were incubated at 37 °C for 5 min. After washing by centrifugation, the fluorescence intensity of the transported polymers was measured. Each value represents the mean ± SD ($n = 6$). (B) Transport of fluorescent polymers into vesicles expressing ABCB1. $^{**}P < 0.01$, compared with the corresponding control group. Each value represents the mean ± SD ($n = 6$). (C) Transport of free fluorescent compounds into vesicles expressing ABCB1. $^{**}P < 0.01$, compared with the corresponding control group. Each value represents the mean ± SD ($n = 6$).

underwent similar transport into the vesicles expressing ABCB1 (Fig. 8B). Free DBD and Nile Red were not, however, transported through ABCB1 (Fig. 8C), indicating that the observed changes in fluorescence did in fact correspond to the transport of the polymers and not to that of dissociated Dox, DBD, or Nile Red. This result indicates that the block copolymers themselves are crucial to their transport by ABCB1, and that the conjugated fluorescent compound is not recognized by ABCB1. The ABCB1 transporter plays a critical role in drug clearance, including urinary excretion in the kidneys, and biliary excretion in the liver [47]. We are currently investigating the role of the ABCB1 transporter in the dynamics and clearance of the polymer and encapsulated drugs *in vivo*.

All of the micelles used in this study showed the same intracellular trafficking and the same proteins were involved in that trafficking, independent of PEG chain length, polymerization degree of P(Asp), and the hydrophobic moiety introduced into the core segment within the range investigated. To determine whether the intracellular trafficking and the molecular mechanism were specific to the block copolymer we used, we tested the more hydrophilic polymer dextran. Dextran is a macropinocytosis marker, and in fact its internalization was inhibited by the macropinocytosis inhibitor EIPA (Supplementary Fig. 7). Because it is possible that macropinosomes directly fuse with NPC1-positive late endosomes [48], dextran can be recycled to the extracellular milieu by NPC1. However, NPC1 was not involved in the trafficking of dextran from the late endosome (Supplementary Fig. 3). Moreover, knockdown of ORP2 and ABCB1 expression, which is involved in block copolymer trafficking, was not involved in the intracellular trafficking of dextran (Supplementary Fig. 5). We also tested a hydrophobic nanoparticle (a polystyrene nanoparticle) and a hydrophilic nanoparticle (a silica nanoparticle) with respect to their intracellular trafficking. The internalization of these nanoparticles was mediated by both clathrin-mediated endocytosis and caveolae-mediated endocytosis (Supplementary Fig. 7) similarly to the block copolymers and micelles we used. However, NPC1, ORP2, and ABCB1 were not involved in the intracellular trafficking of these nanoparticles (Supplementary Figs. 3 and 5). Yet, the efflux of dextran, polystyrene nanoparticles, and silica nanoparticles is controlled by the exocytosis protein snap-25 (Supplementary Fig. 8). Thus, the findings described in this report regarding the intracellular fate of the block copolymers and the intrinsic proteins involved in their trafficking are specific to these block copolymers. From a safety standpoint, further studies are needed to elucidate the physicochemical properties of block copolymers that determine their intracellular trafficking and fate so that we might be able to predict the potential for accumulation of newly developed block copolymers inside cells and/or their efflux from cells. It will also be necessary to elucidate the intracellular trafficking and fate of block copolymers in different cell types.

5. Conclusions

We have characterized here the intracellular trafficking and fate of different block copolymer micelles and their dissociated polymers, from intracellular uptake to extracellular efflux. In addition, we identified three proteins that are involved in the intracellular

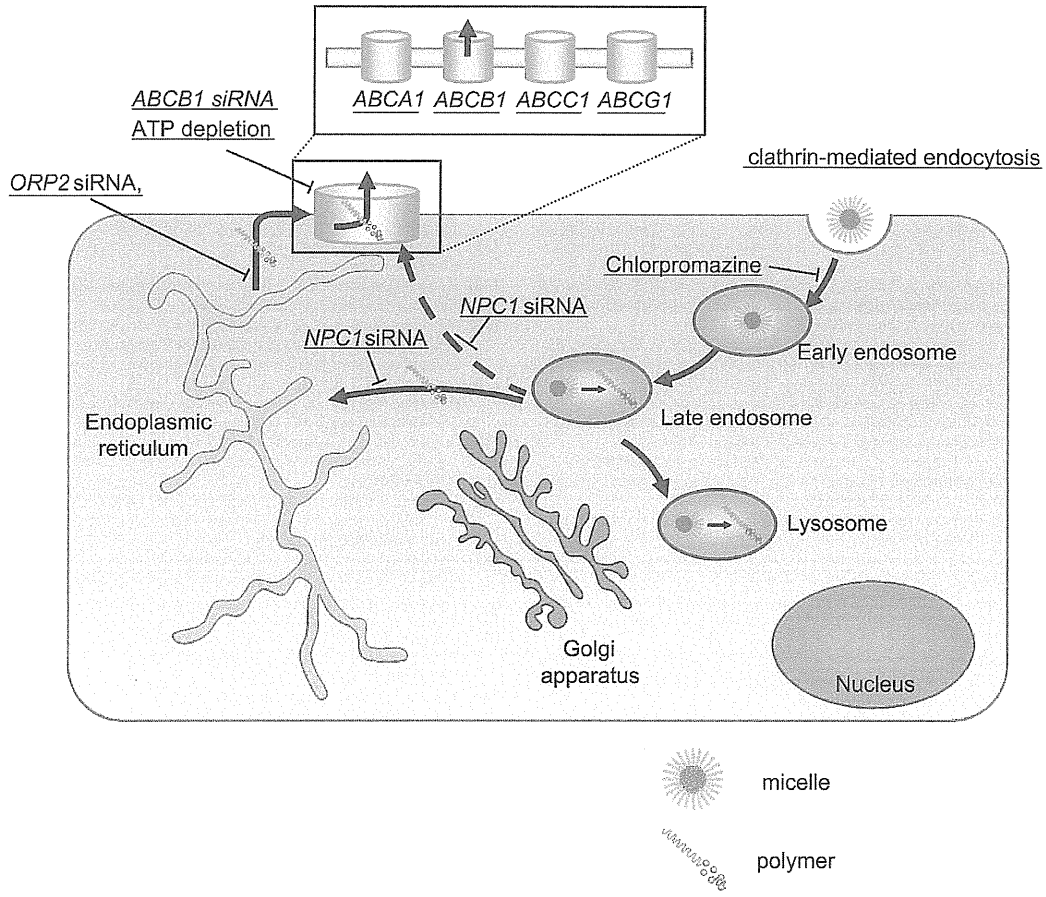

Fig. 9. Predicted mechanism of intracellular trafficking of micelles and polymers used in this study.

trafficking of these polymers: NPC1, ORP2, and ABCB1 (Fig. 9). By using FRET micelles, we showed that the dissociation of the micelles occurs mainly in late endosomes and that NPC1 seems to have a key role in the dissociation of micelles and in the intermembrane transfer of the block copolymers.

Exocytosis is well-known efflux route for nanoparticles internalized by endocytosis. Our study has elucidated a unique trafficking and efflux route for the components of block copolymer micelles in which NPC1 and ORP2 play essential role in the transfer of the block copolymers to their efflux via the transporter ABCB1. This route can prevent the accumulation of components inside the cells after intracellular uptake via endocytosis. Such knowledge may help improve the therapeutic efficacy and minimize the safety risks of block copolymer micelles.

Acknowledgments

This work was supported in part by Public-Private Sector Joint Research on Publicly Essential Drugs from the Japan Health Sciences Foundation, by Health and Labour Sciences Research Grants from the Ministry of Health, Labour and Welfare of Japan, and by JSPS KAKENHI Grant number 24590070. We thank Nippon Kayaku Co. Ltd for providing the block copolymers.

Appendix A. Supplementary data

Supplementary data related to this article can be found at http://dx.doi.org/10.1016/j.biomaterials.2013.11.027.

References

[1] Barenholz Y. Doxil® – the first FDA-approved nano-drug: lessons learned. J Control Release 2012;160:117–34.
[2] Duncan R, Gaspar R. Nanomedicine(s) under the microscope. Mol Pharm 2011;8:2101–41.
[3] Ferrari M. Cancer nanotechnology: opportunities and challenges. Nat Rev Cancer 2005;5:161–71.
[4] Kataoka K, Kwon GS, Yokoyama M, Okano T, Sakurai Y. Block copolymer micelles as vehicles for drug delivery. J Control Release 1993;24:119–32.
[5] Nishiyama N, Kataoka K. Current state, achievements, and future prospects of polymeric micelles as nanocarriers for drug and gene delivery. Pharmacol Ther 2006;112:630–48.
[6] Torchilin VP. PEG-based micelles as carriers of contrast agents for different imaging modalities. Adv Drug Deliv Rev 2002;54:235–52.
[7] Kabanov A, Zhu J, Alakhov V. Pluronic block copolymers for gene delivery. Adv Genet 2005;53:231–61.
[8] Uchino H, Matsumura Y, Negishi T, Koizumi F, Hayashi T, Honda T, et al. Cisplatin-incorporating polymeric micelles (NC-6004) can reduce nephrotoxicity and neurotoxicity of cisplatin in rats. Br J Cancer 2005;93:678–87.
[9] Hamaguchi T, Matsumura Y, Suzuki M, Shimizu K, Goda R, Nakamura I, et al. NK105, a paclitaxel-incorporating micellar nanoparticle formulation, can extend in vivo antitumour activity and reduce the neurotoxicity of paclitaxel. Br J Cancer 2005;92:1240–6.
[10] Koizumi F, Kitagawa M, Negishi T, Onda T, Matsumoto S, Hamaguchi T, et al. Novel SN-38-incorporating polymeric micelles, NK012, eradicate vascular endothelial growth factor-secreting bulky tumors. Cancer Res 2006;15(66):10048–56.
[11] Murakami M, Cabral H, Matsumoto Y, Wu S, Kano MR, Yamori T, et al. Improving drug potency and efficacy by nanocarrier-mediated subcellular targeting. Sci Transl Med 2011;3:64ra2.
[12] Sahay G, Batrakova EV, Kabanov AV. Different internalization pathways of polymeric micelles and unimers and their effects on vesicular transport. Bioconjug Chem 2008;19:2023–9.
[13] Hatakeyama H, Akita H, Harashima H. A multifunctional envelope type nano device (MEND) for gene delivery to tumours based on the EPR effect:

a strategy for overcoming the PEG dilemma. Adv Drug Deliv Rev 2011;63:152–60.
[14] Sakai-Kato K, Ishikura K, Oshima Y, Tada M, Suzuki T, Ishii-Watabe A, et al. Evaluation of intracellular trafficking and clearance from HeLa cells of doxorubicin-bound block copolymers. Int J Pharm 2012;423:401–9.
[15] Nakanishi T, Fukushima S, Okamoto K, Suzuki M, Matsumura Y, Yokoyama M, et al. Development of the polymer micelle carrier system for doxorubicin. J Control Release 2001;74:295–302.
[16] Rejman J, Bragonzi A, Conese M. Role of clathrin- and caveolae-mediated endocytosis in gene transfer mediated by lipo- and polyplexes. Mol Ther 2005;12:468–74.
[17] Perez AP, Cosaka ML, Romero EL, Morilla MJ. Uptake and intracellular traffic of siRNA dendriplexes in glioblastoma cells and macrophages. Int J Nanomed 2011;6:2715–28.
[18] Tomás M, Martínez-Alonso E, Ballesta J, Martínez-Menárguez JA. Regulation of ER-Golgi intermediate compartment tubulation and mobility by COPI coats, motor proteins and microtubules. Traffic 2010;11:616–25.
[19] Uematsu K, Seki N, Seto T, Isoe C, Tsukamoto H, Mikami I, et al. Targeting the Wnt signaling pathway with dishevelled and cisplatin synergistically suppresses mesothelioma cell growth. Anticancer Res 2007;27:4239–42.
[20] Chen H, Kim S, He W, Wang H, Low PS, Park K, et al. Fast release of lipophilic agents from circulating PEG-PDLLA micelles revealed by in vivo forster resonance energy transfer imaging. Langmuir 2008;24:5213–7.
[21] Miller T, Rachel R, Besheer A, Uezguen S, Weigandt M, Goepferich A. Comparative investigations on in vitro serum stability of polymeric micelle formulations. Pharm Res 2012;29:448–59.
[22] Ioannou YA. Multidrug permeases and subcellular cholesterol transport. Nat Rev Mol Cell Biol 2001;2:657–68.
[23] Mineo C, Anderson RG. Potocytosis. Robert Feulgen Lecture. Histochem Cell Biol 2001;116:109–18.
[24] Hölttä-Vuori M, Alpy F, Tanhuanpää K, Jokitalo E, Mutka AL, Ikonen E. MLN64 is involved in actin-mediated dynamics of late endocytic organelles. Mol Biol Cell 2005;16:3873–86.
[25] Xu Y, Liu Y, Ridgway ND, McMaster CR. Novel members of the human oxysterol-binding protein family bind phospholipids and regulate vesicle transport. J Biol Chem 2001;276:18407–14.
[26] Ikonen E. Cellular cholesterol trafficking and compartmentalization. Nat Rev Mol Cell Biol 2008;9:125–38.
[27] Koivusalo M, Jansen M, Somerharju P, Ikonen E. Endocytic trafficking of sphingomyelin depends on its acyl chain length. Mol Biol Cell 2007;18:5113–23.
[28] Hanada K, Kumagai K, Yasuda S, Miura Y, Kawano M, Fukasawa M, et al. Molecular machinery for non-vesicular trafficking of ceramide. Nature 2003;426:803–9.
[29] Hanada K, Kumagai K, Tomishige N, Yamaji T. CERT-mediated trafficking of ceramide. Biochim Biophys Acta 2009;1791:684–91.
[30] Sato K, Nakano A. Mechanisms of COPII vesicle formation and protein sorting. FEBS Lett 2007;581:2076–82.
[31] Townley AK, Feng Y, Schmidt K, Carter DA, Porter R, Verkade P, et al. Efficient coupling of Sec23-Sec24 to Sec13-Sec31 drives COPII-dependent collagen secretion and is essential for normal craniofacial development. J Cell Sci 2008;121:3025–34.
[32] Laitinen S, Lehto M, Lehtonen S, Hyvärinen K, Heino S, Lehtonen E, et al. ORP2, a homolog of oxysterol binding protein, regulates cellular cholesterol metabolism. J Lipid Res 2002;43:245–55.
[33] Hynynen R, Laitinen S, Käkelä R, Tanhuanpää K, Lusa S, Ehnholm C, et al. Overexpression of OSBP-related protein 2 (ORP2) induces changes in cellular cholesterol metabolism and enhances endocytosis. Biochem J 2005;390:273–83.
[34] Hynynen R, Suchanek M, Spandl J, Bäck N, Thiele C, Olkkonen VM. OSBP-related protein 2 is a sterol receptor on lipid droplets that regulates the metabolism of neutral lipids. J Lipid Res 2009;50:1305–15.
[35] Wirtz KW. Phospholipid transfer proteins revisited. Biochem J 1997;324:353–60.
[36] Hsuan J, Cockcroft S. The PITP family of phosphatidylinositol transfer proteins. Genome Biol 2001;2: reviews 3011.1–3011.8.
[37] Ségui B, Allen-Baume V, Cockcroft S. Phosphatidylinositol transfer protein beta displays minimal sphingomyelin transfer activity and is not required for biosynthesis and trafficking of sphingomyelin. Biochem J 2002;366:23–34.
[38] Batrakova EV, Kabanov AV. Pluronic block copolymers: evolution of drug delivery concept from inert nanocarriers to biological response modifiers. J Control Release 2008;130:98–106.
[39] Sugii S, Lin S, Ohgami N, Ohashi M, Chang CC, Chang TY. Roles of endogenously synthesized sterols in the endocytic pathway. J Biol Chem 2006;281:23191–206.
[40] Sahay G, Querbes W, Alabi C, Eltoukhy A, Sarkar S, Zurenko C, et al. Efficiency of siRNA delivery by lipid nanoparticles is limited by endocytic recycling. Nat Biotechnol 2013;31:653–8.
[41] Zhang M, Dwyer NK, Love DC, Cooney A, Comly M, Neufeld E, et al. Cessation of rapid late endosomal tubulovesicular trafficking in Niemann-Pick type C1 disease. Proc Natl Acad Sci U S A 2001;98:4466–71.
[42] Pichler H, Gaigg B, Hrastnik C, Achleitner G, Kohlwein SD, Zellnig G, et al. A subfraction of the yeast endoplasmic reticulum associates with the plasma membrane and has a high capacity to synthesize lipids. Eur J Biochem 2001;268:2351–61.
[43] Hao M, Lin SX, Karylowski OJ, Wüstner D, McGraw TE, Maxfield FR. Vesicular and non-vesicular sterol transport in living cells. The endocytic recycling compartment is a major sterol storage organelle. J Biol Chem 2002;277:609–17.
[44] Némoz-Gaillard E, Bosshard A, Regazzi R, Bernard C, Cuber JC, Takahashi M, et al. Expression of SNARE proteins in enteroendocrine cell lines and functional role of tetanus toxin-sensitive proteins in cholecystokinin release. FEBS Lett 1998;425:66–70.
[45] Bonifacino JS, Glick BS. The mechanisms of vesicle budding and fusion. Cell 2004;116:153–66.
[46] Okayama M, Arakawa T, Mizoguchi I, Tajima Y, Takuma T. SNAP-23 is not essential for constitutive exocytosis in HeLa cells. FEBS Lett 2007;581:4583–8.
[47] Tanigawara Y. Role of P-glycoprotein in drug disposition. Ther Drug Monit 2000;22:137–40.
[48] Kerr MC, Teasdale RD. Defining macropinocytosis. Traffic 2009;10:364–71.

Bull. Natl. Inst. Health Sci., **131**, 2-6 (2013) **Special Report**

革新的医薬品の開発環境整備を目指したレギュラトリーサイエンス研究

川西徹

Regulatory science promoting improvement in developing environment of innovative drugs

Toru Kawanishi

Importance of regulatory science in development of innovative drugs is pointed out by the Council for Science and Technology Policy in the Cabinet Office, and the pharmaceuticals-related divisions in the NIHS have begun the regulatory science research for promoting improvement in developing environment of innovative drugs since 2012. Nano-medicines, fully engineered protein drugs, nucleic acid drugs, and gene therapy drugs have been selected as innovative drugs, and the point-to-consider documents for evaluating mainly quality and non-clinical safety of these drugs will be developed. In addition, the conditions for the first-in-human trial will be also proposed, especially from the standpoints of quality and non-clinical safety evaluation.

Keywords: Nano-medicine, Nucleic acid drug, fully engineered protein drug, gene therapy drug

1．はじめに —革新的医薬品のレギュラトリーサイエンス（RS）研究の必要性—

医薬品，医療機器は(1)生命に直接関わる；(2)多くの国で公的医療保険制度により費用負担される公的な性格を有する；(3)それゆえ厳しい規制下にあり，承認基準および市販後においても監視が厳格　という特殊な工業製品である．そのため，近年開発経費の高騰が著しく，新薬の開発が困難になっていることが世界的に指摘されている．一方我が国における医薬品開発環境の問題として，アカデミア等における創薬関連の基礎研究レベルは高く医薬品等のシーズは数多く発見されているにもかかわらず，それにみあった日本発の新薬の開発例が少ないこと，さらに医薬品，医療機器の実用化のスピードが欧米に比べて遅く，欧米で承認されていても我国での承認が遅い，いわゆるドラッグラグ，デバイスラグが問題となっている．このような我が国における医薬品の製品化のスピードの遅さの主要な原因の一つとして，製品化及び承認申請・審査の過程のシステム整備が不十分であることが指摘されている．

To whom correspondence should be addressed to
Toru Kawanishi; Director of National Institute of Health Sciences, 1-18-1 Kamiyoga, Setagaya-ku, Tokyo 158-8501, Japan; Tel: +81-3-3700-1141 ext. 200; Fax: +81-3-3700-1340; E-mail: kawanish@nihs.go.jp

この状況を打開するために，日本発の医薬品，医療機器，さらに再生医療製品の開発を効率的・効果的に行うためのRS研究を充実・強化し，革新的医療技術の適切な評価，根拠に基づいた審査指針や基準策定等の作成の推進が，“第４期科学技術基本計画（平成23年８月）”および“科学技術イノベーション総合戦略～新次元日本創造への挑戦～（平成25年６月７日）”等において科学技術政策の最重要課題の一つとしてあげられている．

この施策を実現するため，国立医薬品食品衛生研究所では，平成24年度から以下の革新的医薬品，医療機器，および再生医療製品の評価技術開発研究への取り組みを開始している．そこで本稿では，革新的医薬品の評価技術開発研究に絞って，国立衛研における具体的な取組の目的，および成果目標をまとめる．

2．国立医薬品食品衛生研究所における“革新的医薬品の開発環境整備を目指したRS研究”とは

(1) 革新的医薬品とは

“第４期科学技術基本計画”あるいは“科学技術イノベーション総合戦略～新次元日本創造への挑戦～”において，「革新的医療技術の研究開発・実用化の推進及び評価手法の確立」が対象とする国立衛研がかかわる「革新的医療技術」としては，まず再生医療製品あるいは医療機器があげられるだろう．それでは，国立衛研が関わる革新的医薬品については，どのような医薬品が対象と